

Norwegian University
of Life Sciences

Master's Thesis 2018 30 ECTS

Faculty of Environmental Sciences and Natural Resource Management

Application of Waterborne Electrical Resistivity Tomography and Ground Penetrating Radar in the Delta Area of Numedalslågen, Norway

Vilde Jørdre Øybekk

Environment and Natural Resources

PREFACE

This master thesis is the final project of my five years as a student at Norges miljø- og biovitenskapelige universitet (NMBU). There are many people who have supported me in this process. I would first like to thank my supervisor Mona Henriksen! You have been encouraging, supportive and found solutions to the challenges I have had with my thesis. Thanks to Jürgen Scheibz, my co-supervisor at NGI for giving me the opportunity to work with this project and learn more about ERT (and geophysics in general), through guidance and feedback during my work. Several other employees at NGI have also helped me. Thank you to Sara Bazin for help and guidance with processing and interpretation of the ERT data. I am very grateful! I had four very nice days of fieldwork in Larvik with Helgard Anschütz and Asgeir Olaf Kydland Lysdahl. The two of you and Regula Frauenfelder also helped with processing of the ERT data that I could not have managed without. Leif Vidar Jakobsen at NMBU helped me with collection and processing of GPR data. Thanks to all of you! I would also like to express my gratitude to NGI for funding the project.

I would also like to thank my fellow students at NMBU for five amazing years. The student life in Ås is really one of a kind, with so many people contributing and working hard for each other. To all the women in Pikekoret IVAR: these years would not have been the same without you. Thanks to my parents for support and (the good) advices during my years as a student. Last, but not least: thank you to all my friends for just being the best!

Norges miljø- og biovitenskapelige universitet

Ås, 15.06.2018

Vilde Jørdre Øybekk

ABSTRACT

Two non-invasive geophysical methods have been tested in the lowermost reaches of the river Numedalslågen, Southern Norway. The aim were to estimate thickness of sediments, possible layering and the depth to the bedrock. Waterborne electrical resistivity tomography (ERT) measurements were conducted in brackish water above the delta. Several lines of ERT data were collected by towing an electrode streamer by boat. The data were processed in RES2DINV. Processing of the ERT data gave resistivity values mainly ranging from approximately 20 to 60 Ωm . This can be interpreted as clay rich sediments, when seen in context of the settings and knowledge about the geomorphology of the area. However, challenging conditions during the survey gave data and results that were difficult to interpret further. One standard resistivity value for the water body based on conductivity measurements and editing of the data to include bathymetry data were tried to improve the results. Nevertheless, few measured data points compared to a high number of model blocks, high RMS errors and vertical rather than horizontal sections in the processed data gave little confidence in the results. Ground penetrating radar (GPR) data were collected along three profiles at a beach in the SE end of the delta. Antennas of 50 megahertz were used to map deposits and subsurface structures, resulting in GPR profiles with reflections mainly interpreted as sand and a maximum penetration depth of 20 meters. Reflection free parts were interpreted as clay rich sediments or sediments with brackish groundwater. Despite challenges with processing of data and interpretation of results, the methods should be considered suitable for the target of the study. The settings were demanding, especially for the ERT, and this is reflected in the results.

SAMMENDRAG

To ikke-invasive geofysiske metoder har blitt testet i og langs utløpet til Numedalslågen, sør i Norge. Målet var å estimere mektighet av sedimentene, mulige lagdelinger og dybde til fjell. Vannbåren Elektrisk Resistivitets Tomografi målinger ble utført i brakkvannet over deltaet. Flere linjer med ERT data ble samlet inn ved at en elektrodekabel ble tauet med båt. Dataene ble prosessert i RES2DINV. Prosessering av ERT dataene ga i hovedsak resistivitetsverdier mellom 20 og 60 Ωm . Dette kan tolkes som at sedimentene er rike på leire, særlig sett i sammenheng med området og dets geologiske utvikling. Utfordrende forhold under feltarbeidet gjorde det derimot vanskelig å tolke data og resultater videre. Forsøk på å forbedre dataene ble gjort, som ved å for eksempel å sette en resistivitetsverdi som standard for vannet og endre redigering av batymetridata. Likevel gav prosesseringen lite pålitelige resultater. Georadardata ble samlet inn langs tre profiler på stranda i SØ-retning for deltaet. 50 megahertz-antennene ble brukt i forsøket på å kartlegge løsmasser og strukturer under overflaten. Det resulterte i georadarprofiler med refleksjoner som i hovedsak ble tolket som sand. Signalet fra georadaren nådde dyp på maksimum 20 meter. Refleksjonsfrie områder ble tolket som sedimenter rike på leire eller med innhold av brakt grunnvann. På tross av utfordringer med prosessering av data og tolkning av resultatene, bør metodene anses som passende for studiets mål. Krevende forhold, særlig under innsamlingen av ERT data, er reflektert i resultatene.

CONTENTS

1. Introduction	1
1.1 Purpose and background.....	1
1.2 Climate change	2
1.3 River dynamics, sediment transport and stability.....	3
1.4 Literature research	6
1.4.1 ERT	6
1.4.2 ERT results with interpretations	8
1.4.3 GPR.....	9
2. Investigation area	10
3. Methods	15
3.1 Electrical resistivity tomography.....	15
3.1.1 Theoretical background.....	15
3.1.2 Advantages and limitations.....	19
3.1.3 ERT data collection and processing.....	20
3.2 Ground penetrating radar	23
3.2.1 Theoretical background.....	23
3.2.2 Advantages and limitations.....	26
3.2.3 GPR data collection and processing.....	27
4. Results	29
4.1 ERT results	29
4.2 GPR results	39
5. Discussion	46
5.1 Discussion of ERT data	46
5.3 Discussion GPR data	50
5.4 Geology and risk of erosion.....	52
6. Conclusion.....	53

7. References	54
8. Appendices	60
Appendix A: Catchment of Numedalslågen	60
Appendix B: The development of Revet	61
Appendix C: Nautical chart of study area	62
Appendix D: GPR profiles	63

1. Introduction

1.1 Purpose and background

This master thesis is written as a final assignment in the master's program 'Environment and Natural Resources' at the Norwegian University of Lifesciences (NMBU). It is written in cooperation with the Norwegian Geotechnical Institute (NGI), as a part of the 'MERRIC project' (Multi-scale Erosion Risk under Climate Change), with funding from NGI and NFR (The Research Council of Norway). The MERRIC project is defined as a part of monitoring, warning and non-physical mitigation measures (NGI, n.d.).

The aim of this project is to map sediments by the use of geophysical methods. The results will be used to interpret thickness of deposits and possible layers in and along the lowermost reaches of the river Numedalslågen in Larvik, Norway. Waterborne Electrical Resistivity tomography (ERT) were used in the delta area of the river and ground penetration radar along the river. By using geophysical methods and comparing the results with already existing maps and general knowledge about the geomorphology in the area, the erosion risk is also discussed.

There are several geophysical methods applicable for investigating geological structures or depth to bedrock, e.g. gravity, magnetic, resistivity, ground radar or seismic reflection survey techniques (Table 1.1 in Sharma (1997)). However, the choice of method should give high resolution data in small-scale surveys and preferably provide data where layers of sediments can be distinguished from one another. It was also important to use a method that met the requirements of being applicable in waterborne surveys, to be able to map the sediments of the delta.

1.2 Climate change

Effects of climate change is an increasing threat to settlements and land use. Changes in precipitation patterns, more frequent flooding and sea level rise are examples of natural hazards that possibly can have significant impact on the landscape. An increased risk of erosion of riverbanks and coastal zones are among the responses that can be expected of changes in the hydrological cycle. Knowledge of geology and stability in soils and sediments is therefore crucial to protect e.g. buildings, infrastructure and agricultural land. Erosion can be caused by several natural processes, e.g. flooding caused by rapid snowmelt or high intensity rainfall, frequent freeze and thaw episodes, or changes in tides or wave energy.

Reliable instrumental meteorological data from more than the last 150 years show a changing trend in the hydrological cycle (Hanssen-Bauer et al., 2017). These data and estimates of variables in the water balance are useful to get an understanding of the changing climate. An estimate of annual mean precipitation in Norway is set to be approximately 1600 mm (for 1971 – 2000). This is an increase of 18% from 1900 (Hanssen-Bauer et al., 2017). Runoff rates are and have been relatively stable at around 1100 mm/year, which suggest an increase in evaporation rates (500mm/year today). This can be explained by higher atmospheric temperatures (Hanssen-Bauer et al., 2017). An increase of the *amount* is not the only change in precipitation patterns. When ‘reference periods’ of 30 years are compared in the report ‘Climate in Norway 2100’, changes in the *type* of precipitation could be even more important. It is concluded that the summers are getting dryer, and the springs wetter (Hanssen-Bauer et al., 2017). More precipitation falls as rain, less as snow, with an increased frequency of high intensity rainfall. This gives a higher runoff rate in the spring, with more discharge of water to rivers and an increased possibility of spring floods (Hanssen-Bauer et al., 2017). Average annual temperature and precipitation for Larvik in the period 1971 – 2000 were 6.7 °C and 1050 mm/year, according to Norsk Klimaservicesenter (2015). In the whole county of Vestfold it should be expected an annual increase of 10 % for precipitation towards 2100, with higher frequencies of extreme events and high intensity rainfall (Norsk Klimaservicesenter, 2015).

Investigations of the subsurface structures of deltas, riverbanks and coastal areas can give better knowledge of the erosion risk. The composition and thickness of soils and sediments can increase the understanding of the possibility for erosion in an area, which is important for safe planning of future land use.

1.3 River dynamics, sediment transport and stability

River dynamics and sediments transport is an important relationship for erosion and deposition. The eroding forces of a river is highly dependent on the water discharge, Q , the rivers cross section and the gradient of the terrain. These variables are reflected in the velocity of the river. Grain sizes and packing efficiency of the deposits in the river is also important (Jørgensen et al., 1997). Erosion, transportation and deposition will be very different in a narrow, steep valley, compared to a wide valley with a gentle gradient. A steep and narrow slope typically results in a high velocity river with coarse sediments or directly on the bedrock. In a wider valley with low gradient, the river is likely to meander, and this results in different sediment transport. A meandering river erode sediments in cut banks where the velocities are high, compared to the point bars where sediments are deposited (Jørgensen et al., 1997; NVE, 2010).

The transportation of sediments is dependent on the velocity of the river. With higher velocities, the competency of the river increases, which is reflected in a sediment transport with increasing grainsizes (Økland & Økland, 2006). With a declining gradient in the terrain, the response from the river will be a slower running water stream. Fine grained sediments as clay, silt or fine sand is likely to be transported far, but heavier material as coarse sand and gravel will be deposited in and along the river. Equation 1.1 below show the relationship of transported material, where the diameter of the transported material (d) is determined by the velocity of the water, v_c and the degree of sorting and rounding of the material, k_d :

$$d = k_d \times v_c^2 \quad (1.1)$$

As an example deposits that are well sorted and rounded will have a k_d value of approximately 4 (Jørgensen et al., 2013, p. 50). Periods with increased rainfall or runoff to the river is likely to give a stronger water flow of the river and a change in the erosion, transport and deposition pattern of the sediments. Erosion and deposition can also be explained by the Hjulström curve (figure 1).

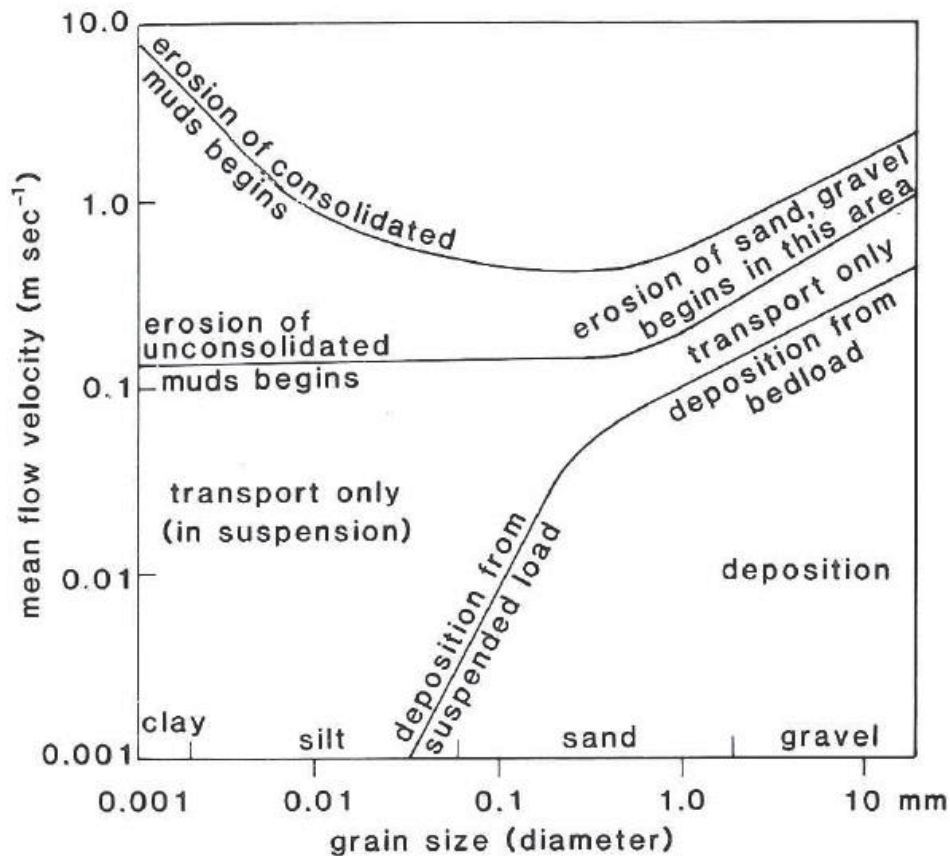


Figure 1: The Hjulström curve show how velocity and diameter of grain sizes determine if sediments will be eroded, transported or deposited. From Tucker (1991).

The transportation of sediments is divided in four categories. Traction and saltation is movement of the sediments along the bottom of the river, suspension is the movement of fine particles in the water and solution is the movement of ions in the water. Fine sand will typically bounce along the bottom of the river by saltation, but clay and silt particles are carried in suspension by the water stream (Jørgensen et al., 1997; Økland & Økland, 2006). The material transported by saltation will be deposited when the velocity of the river stream is decreased in a ratio that reflects the degree of sorting and rounding of the material. Silt and clay particles on the other hand, is dependent on flocculation to precipitate and build up large particles heavy enough to be deposited (Tucker, 1991). This happens when the suspended particles reach the river mouth by the sea, and the salts from the seawater reacts with the silt and clay particles. Alternating layers or mixed deposits of well sorted sand with fine marine sediments as silt and clay is expected to be found in the delta (Jørgensen et al., 1997).

Stability in sediments and risk of erosion depends on several factors. Friction between particles in sediments or soils give a certain degree of stability, dependent on the sorting of the material and grain sizes. In soils with a high content of fine grains, cohesion can increase the friction. These factors are important for the stability in a slope gradient (NVE, 2010). External forces can change the stability in the sediments and increase the risk of erosion. Change in water saturation in sediments or change of weight along the slope can trigger erosion or slides (De Blasio, 2011). Increase in water discharge of a river or changes in sea levels can affect the stability and increase the erosion risk.

1.4 Literature research

1.4.1 ERT

Waterborne electrical resistivity tomography (ERT) was considered as a possible method to investigate delta sediments. A literature research has shown that ERT is a widely used geophysical method, which through imaging and mapping of structures beneath the ground gives a picture of the subsurface. Interpretation of data can give an understanding of the layers of sediments or geological structures both on land and in aquatic environments (Dahlin et al., 2014; Maillet et al., 2004). It is a relatively common method used in land geophysics, such as mapping of subsurface structures, pollution in sediments or groundwater flow (Cassiani et al., 2006; Daily et al., 2004). ERT is a method that is still being tested and developed to better understand the range of possible use in aquatic surveys (Crook & Rucker, 2017).

ERT has successfully been used in surveys focusing on submarine groundwater discharge (SGD), both with submerged stationary cables mapping differences in resistivity and continuous resistivity profiling (CRP). It gives an understanding of structures in submarine sediments and bedrock based on changing values in resistivity (Befus et al., 2014).

Submerged stationary ERT has been used with focus on spatial and temporal distributions of SDG. In Day-Lewis et al. (2006) it is stated that CRP is useful when investigating structures and lithology of the substructures, giving estimates of the water depth and the bedrock surface. Interpretation of differences in resistivity can be used to identify areas and layers of sediments saturated with freshwater in the SDG zone (Day-Lewis et al., 2006). Other studies have in addition used natural occurring isotopes in the groundwater as tracers (e.g. the ^{222}Ra -isotope) to easier be able to interpret changes in mixing zones in SGD studies (Breier et al., 2005; Cardenas et al., 2010; Swarzenski et al., 2007). The resistivity in subsea sediments and bedrock is mapped and compared with changes in conductivity in mixing zones between fresh and saline groundwater.

In addition to studies with focus on SGD, waterborne ERT has also been used to plan dredging of the Panama Canal (Rucker et al., 2011), in archaeological studies to find submerged targets of metal (Passaro, 2010) and to map submarine geology and its structures in an area (Colombero et al., 2014; Crook & Rucker, 2017). In Epting et al. (2012), it is used a 3D diagram based on several ERT profiles and lithostratigraphic information from boreholes to make a model of the subsurface beneath a river. Interpretation of variations in resistivity

and sediments from the borehole-cores gives an understanding of the thickness of sediments and rock structures.

In Dahlin et al. (2014) underwater ERT was used in a project for a new line for Stockholm Metro. By using submerged cables, the thickness of bottom sediments, rock quality and weak zones in bedrock were investigated. Records of the water depth were included in the processing of ERT data, so the water resistivity could be integrated in the model. The data resulted in a model with several layers of different resistivity, interpreted to be superficial layers of sediments overlying the bedrock (Dahlin et al., 2014). In Clémence et al. (2017) time-lapse underwater 3D ERT was used to monitor a brine injection. It gave insight in solute transport in the sediments of a stream bed, and spatial distribution of tracer fluxes. Transport and persistence of the brine injection, monitored by ER, gave an understanding of heterogeneities and hydraulic conductivity of the sediments in the monitored area.

Most of the studies have concluded with ERT being a successful method for use in aquatic environments, but often in combination with other methods as salinity tests, tracer tests or data such as geological maps or borehole logs (Clémence et al., 2017; Dahlin et al., 2014; Epting et al., 2012).

1.4.2 ERT results with interpretations

Results of waterborne ERT data from the literature research is presented in table 1. The resistivity values with interpretations can be used for comparison of new ERT data.

Table 1: Main findings of resistivity values from waterborne ERT surveys and a brief explanation of the interpretations from a selection of papers.

Publication	Main findings resistivity	Interpretations
Clémence et al. (2017)	Resistive top layer ($> 200 \Omega\text{m}$) Conductive layer ($< 10 \Omega\text{m}$) Bottom layer ($40\text{--}80 \Omega\text{m}$)	Silt and gravel Layer with clay Limestone (bedrock)
Colombero et al. (2014)	Uniform top layer ($10 - 20 \Omega\text{m}$) Lakebed, varying resistivity ($90 - 300 \Omega\text{m}$)	Lacustrine sediments with clay Consolidated silty sand ¹
Crook et al. (2008)	Thin conductive top layer ($4\text{--}75 \Omega\text{m}$) Resistive layer ($95 - 1500 \Omega\text{m}$) Conductive layer ($10 - 75 \Omega\text{m}$)	Thin soil in river bottom Alluvial gravel Underlying weathered chalk
Dahlin et al. (2014)	Conductive top layer ($<12 \Omega\text{m}$) Part of ERT line ($12\text{--}36 \Omega\text{m}$) Deep, resistive layer ($100 - 1000 \Omega\text{m}$)	Unconsolidated sediments Fractured and weathered rock Bedrock, varying composition and weathering.
Epting et al. (2012)	Resistive surface layer ($100 - 500 \Omega\text{m}$) Conductive bottom layer ($10 - 40 \Omega\text{m}$)	Streambed sediments ² Corresponding to the bedrock
Huntley et al. (2017)	Thick conductive layer ($<50 \Omega\text{m}$) Underlying resistive layer ($100\text{--}500 \Omega\text{m}$) Bottom layer, highly resistive ($>1000 \Omega\text{m}$)	Clay Till Underlying bedrock
Nyquist et al. (2008)	Resistive surface layer ($100 - 400 \Omega\text{m}$) Conductive middle layer (20 to $100 \Omega\text{m}$) Resistive bottom layer ($100 - 450 \Omega\text{m}$)	Streambed sediments Clay sediments Carbonate bedrock
Sebok et al. (2018)	Resistive top layer ($70\text{--}120 \Omega\text{m}$) Middle layer ($40 - 70 \Omega\text{m}$) Conductive bottom layer ($<40 \Omega\text{m}$)	Moraine sand Moraine clay Clay

1: “Over-consolidated silty sand with rare clasts (submarginal melt-out-till), locally covered by silty sand with gravel (marginal glaciogenic deposits forming kames and kame-moraines)” (Colombero et al., 2014).

2: Streambed sediments horizontally, two vertically structures interpreted to be karst/fault zone (Epting et al., 2012).

1.4.3 GPR

Ground penetrating radar (GPR) is another common geophysical method, used for mapping geological structures and distribution of sediments in the subsurface in terrestrial environments. A wide range of literature concludes the method as suitable to collect information about layers and structures in sandy sediments like aeolian, coastal or fluvial environments (Bristow & Jol, 2003). GPR was used in combination with borehole data to characterize types of sediments, deposition and relate the findings to depositional processes of a delta in Eilertsen et al. (2011). Layers of sand and clay could be distinguished from each other, and GPR seemed like a helpful tool in giving an impression of subsurface layers. In a publication by Vandenberghe and van Overmeeren (1999), GPR data was compared with geomorphological data and sediments from drilling of sediments in paleochannels in the Netherlands. The GPR results gave distinct differences in the reflection patterns, depending on the types of river systems. In combination with knowledge about the sediments from drilling and geomorphological data, it could be interpreted whether the sediments were deposited in meandering or in braided rivers (Vandenberghe & van Overmeeren, 1999).

In the investigation of weaknesses in subsurface structures, GPR has been applied as a method to detect animal burrows in river embankments (Di Prinzio et al., 2010). Levees are important in protection of land that are under the risk of flooding, and should be investigated regularly, to detect structures like tunnels, holes or other weaknesses. GPR is a cost-effective method which gives high resolution and detailed data. Air filled tunnels and holes can be told apart from the sand and clay rich soils in the levees (Di Prinzio et al., 2010). The existing literature on the use of GPR as a method to map sandy soils and structures near rivers seems to conclude with the method being sufficient to distinguish layers, structures and voids. In combination with other data, methods or observations, the interpreted data seems to give a good impression of the subsurface.

2. Investigation area

Fieldwork was carried out in Larvik, a town and municipality in the southern part of Norway (figure 2), in the lower reaches and the river mouth of Numedalslågen. Numedalslågen is Norway's third longest river. It ranges from Hardangervidda, runs through the valleys Numedal and Lågendal north and south of Kongsberg, respectively before discharging in the Larvik fjord. The long river course of 250 km used to be important for the transport of timber and has been considered as valuable for migration of anadromous fish like salmon. In modern times dams has been built and developed for hydropower, and the migration of salmon is limited (Thorsnæs & Heggstad, 2017).

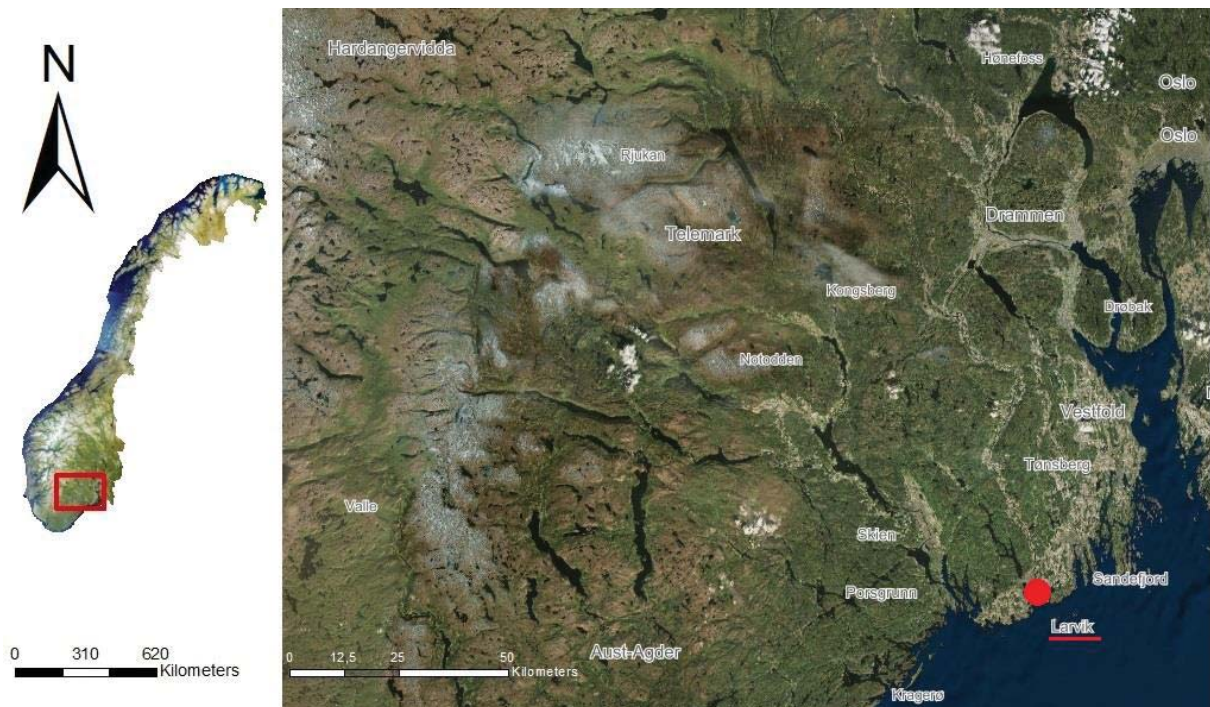


Figure 2: Map of Norway and the south-eastern part of Norway. Larvik is marked in red. (Maps from Kartverkets service GeoNorge (n.d) (left) and ArcMap's basemap (right), made in ArcMap).

The catchment area of Numedalslågen (figure 3) is 5547 km², which is relatively small considering the length of the river. The river course run through several types of bedrock. Hardangervidda consists of magmatic and metamorphic rocks like granites and gneiss, followed by sedimentary and metamorphic sandstones, quartzite and gneiss dominating along the river valley in Buskerud. Igneous syenites and monzonite are more common closer to the river mouth (Berthelsen & Sundvoll, 1996; Dons & Jorde, 1978; Sigmond, 1998). These rocks have been eroded by ice and water through thousands of years, which has formed the

valley as it is known today. With the exception of a few bedrock thresholds, the valley floor is filled with sediments, mainly of marine and fluvial origin south of Kongsberg (Jørgensen et al., 1997).

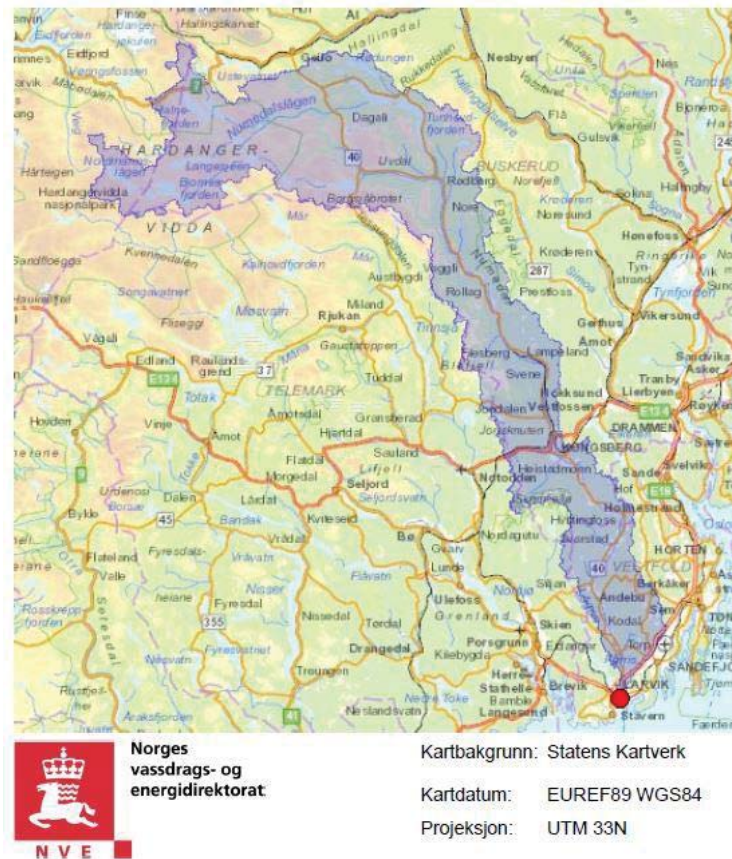


Figure 3: Cathment of Numedalslågen (From NVE, n.d.).

The loose deposits along the river course are strongly connected with the last deglaciation. As the ice retreated, ablation of rocks of different grain sizes from the ice would leave the landscape covered with till. During temporary stops and even ice advances of the generally retreating ice, the till would be deposited as a moraine (Jørgensen et al., 1997). The most prominent moraine in the region is the Ra moraine, it is seen as a green band in SW-NE direction in figure 4. In Jørgensen and Sørensen (1979), studies of the deglaciation is describes with retreats and readvances during Allerød and early Younger Dryas (11 000 – 10 700 B.P). The ice is assumed to have had its last retreat from the Ra 10 600 years ago (Jørgensen & Sørensen, 1979). This is based on dating of marine shells in glaciomarine clays below the till at other locations in Vestfold Vestfold (10 650 ± 150 B.P. in Sandefjord and 10 850 ± 150 B.P. in Tønsberg) (Jørgensen & Sørensen, 1979). The further retreat of the glacier in N-NW to Kongsberg is interpreted by glaciofluvial deposits in the valley.

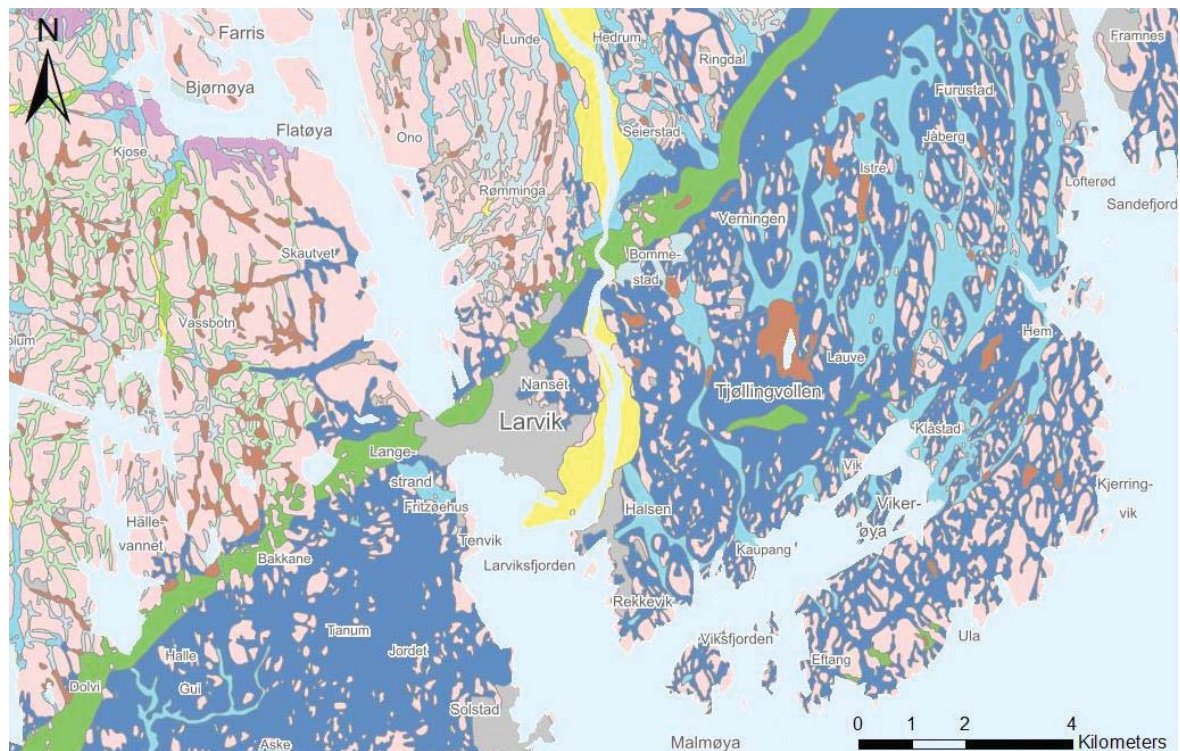


Figure 4: Map showing the deposits in the area of Larvik. The light blue markings are marine deposits, dark blue are beach deposits, yellow markings are fluvial deposits and pink is bedrock with thin or no soils. The green band is the Ra (terminal moraine) (From NGU WMS (NGU, n.d)).

As the ice margin started retreating, the pressure of the crust decreased and led to an isostatic uplift. High sea levels would follow the retreating ice front and flood the land. Several of today's valleys were fjords, including Lågendalen ("Lågenfjorden") with deposition of marine silt and clay as far inland as Kongsberg (Jaksland, 2014; Jørgensen et al., 1997). The marine limit in Larvik is approximately 155 m.a.s.l. according to Jørgensen and Sørensen (1979). In a revised shore-line displacement curve in Sørensen et al. (2014), calibration of old data and additional analysis of sediments and marine fossils supports gives an understanding of the retreat and following crustal rebound. From the shore-line curve, the crustal rebound is interpreted to 4 cm/year 12 200 calibrated years B.P. The rebound increased to 8.8 cm/years 10 900 cal. years. B.P, before a decrease to approximately 1 cm/year 8000 cal. years B.P (Sørensen et al., 2014).

Following the uplift of the land, deposition of marine clays and fluvial sediments and erosion have been dominating process in Lågendalen (Sørensen, 1982). Examples are several fluvial erosion brinks and drainage channels in the deposits along the lowermost reaches of the river (Olsen & Løwe, 1984). With the isostatic uplift, the base level for erosion changes and the river form terraces in the landscape as it erodes deeper in the fluvial deposits. Today the lower reaches of the river is shallow, with depths of approximately 2-3 meters (Kartverket, n.d. a))

High levels of precipitation and quick melting of snow on Hardangervidda has previously exposed the catchment of Numedalslågen to several flood, e.g. in 1987, 2000, 2007 and 2015 (Harbitz et al., 2016). High intensity rainfall in both 2007 and 2015 caused flooding of agricultural land near the lowermost reaches of Numedalslågen (Norsk Klimaservicesenter, 2015). The flood in 1987 was caused by a storm flood (storm surge). An estimate based on interpretation of old data indicates that the storm flood caused water levels of 160 cm higher than the tidal water level (Harbitz et al., 2016, p. 94) . According to the service of water level and tidal information provided by Kartverket (n.d. b)), the highest tides from the area between Revet and Hvittensand is +25 cm, compared to a NN2000 of 0 cm ('Norwegian Normal Null 2000' NN2000 of 0 cm equals 0 m.a.s.l. for a nautical chart). Highwater with 1 and 5 years return periods are 85 and 104 cm (Kartverket, n.d. b)).

The study site is in the river mouth of Numedalslågen, Larvik (figure 5), where the freshwater from the river mixes with the salt water from the fjord. When the river reaches the Larvik fjord, most of the transported sediments are deposited and a delta has been built up over time. With depths up to 90 meters, the fjord is deep compared to the river and delta which creates a steep gradient. Based on information from maps, a depth of 2-3 m is expected in the lower reaches of the river (Appendix C). Bathymetry data indicating indicates a trench near Revet with depths up to 6 meters can imply a varying topography at the delta top (GeoNorge, n.d). Nevertheless, a steep gradient between the delta and the fjord is expected, with depths shallower than 10 meters at the delta top and deeper than 60-70 meters in the fjord.



Figure 5: Aerial map of Larvik. The river Numedalslågen flows from the N and deposit sandy sediments in the investigation area (in the red square) (From Kartverkets WMS (GeoNorge, n.d)).

The beach Hvittensand located on the SE side of the river mouth is a terrestrial part of the delta. Sand is deposited between bedrock outcrops, and partly covers a relatively steep hill. A long spit extends the beach in the SW end. North of Hvittensand and the delta, one can find the harbour of Larvik, Revet. Old maps and aerial photos (appendix B) show natural changes in the deposition of sediments and later a manmade development in the extension of Revet. Maps and bathymetry data indicate some erosion and re-deposition of the fluvial sediments in the delta during seasons and decades. The accuracy of the old maps is hard to determine, but the maps indicate changes. The development of the harbour includes extensions of foundations and protective barriers, as boulders, coarse sediments and concrete to protect SE side of the harbour against erosion.

3. Methods

3.1 Electrical resistivity tomography

3.1.1 Theoretical background

Electrical resistivity tomography measures variations in resistivity of the subsurface. A direct current is injected to the ground through a pair of current electrodes, and the reflected current is measured by pairs of potential electrodes. Figure 6 show the principle of the method.

Differences in resistivity in soils, sediments and bedrock can be used to interpret structures and layers. Resistivity (ρ), is a measure of how strongly a material opposes to the flow of an electric current (Holtebekk, 2017). The resistivity is defined in equation 2.1, where A is as the cross-sectional area and l is the length of the material:

$$\rho = R \times \frac{A}{l} \quad (2.1)$$

The resistance R is described by Ohm's law in equation 2.2. The current I is measured in Ampere and the potential difference, or voltage, V is measured in Volts. The resistance is measured in Ohms, Ω . The electrical current is a movement of charge and follow Ohm's law:

$$R = \frac{V}{I} \quad (2.2)$$

Resistivity of soils and sediments can be described by equation 2.3. This is known as the general form of Archie's law, or the formation factor, F (Sharma, 1997). The relationship of resistivity of earth materials and the resistivity of the pore water ρ_w , is dependent on porosity ϕ and the constants a (coefficient of saturation) and m (cementation factor):

$$F = \frac{\rho}{\rho_w} = a\phi^{-m} \quad (2.3)$$

The Earth has a natural resistivity due to different properties of minerals, bedrock and soils or organic layers in the subsurface. The degree of water saturation in the soil will also have an impact on the resistivity and electrical properties of the subsurface. So will the distribution of air, water and soil particles, in addition to the amounts of dissolved salts in a sediment. Solid rocks will in general have a higher resistivity than deposits, and fresh water will be more resistive than saltwater (Figure 7).

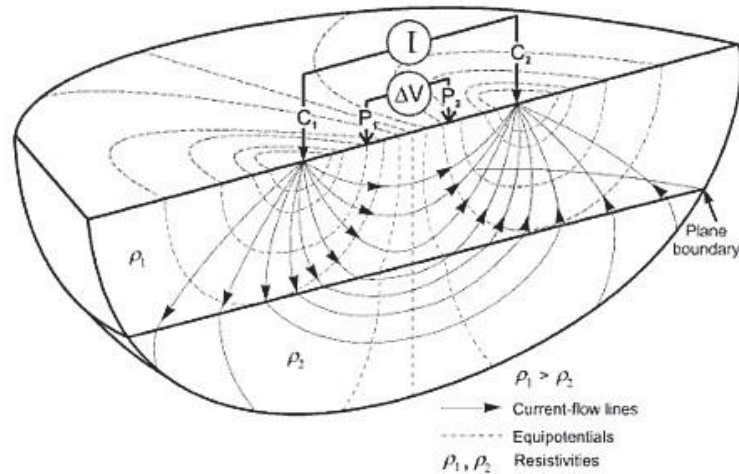


Figure 6: Principles of ERT with current flow lines through current electrodes and equipotential lines through potential electrodes. From Knödel et al. (1997).

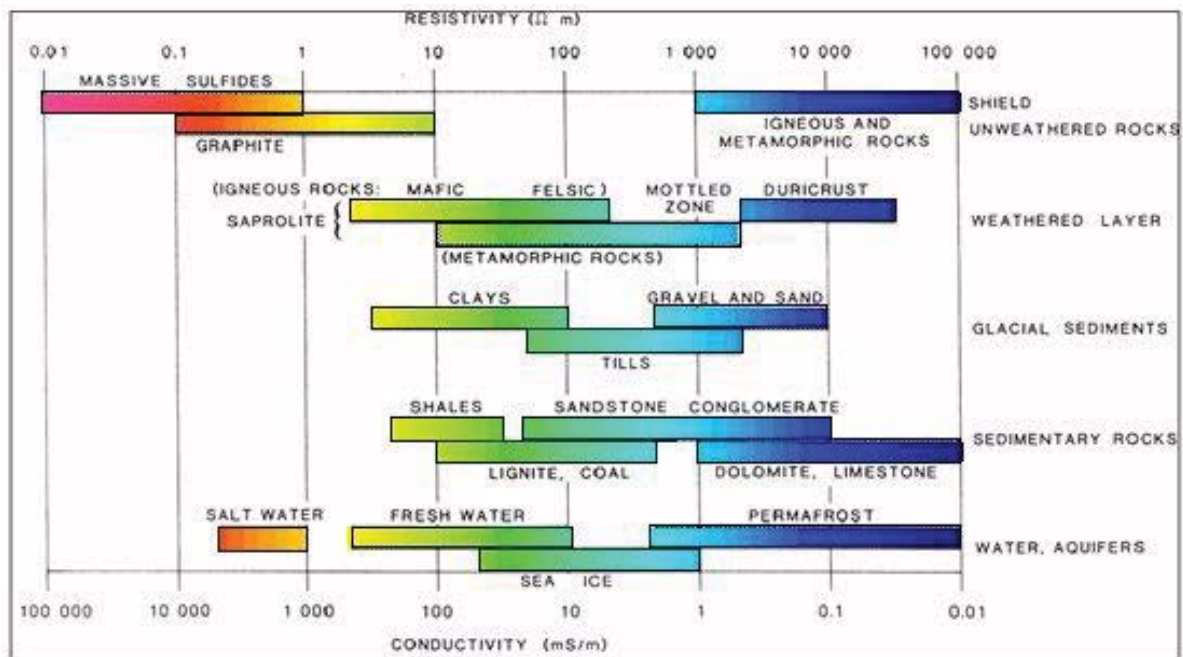


Figure 7: Ranges of resistivity and conductivity for different types of rocks, sediments, elements and water. After Palacky (1987).

The electrodes that are used to inject a current and measure the potential resistivity, can be arranged in different ways. There are several variations of the arrays, but among the most common ones are Wenner, Schlumberger, pole or dipole, or combinations of these (figure 8). Each array type have different characteristics concerning depth of investigation, sensitivity to changes in subsurface resistivity, data coverage and signal strength (Loke, 2016).

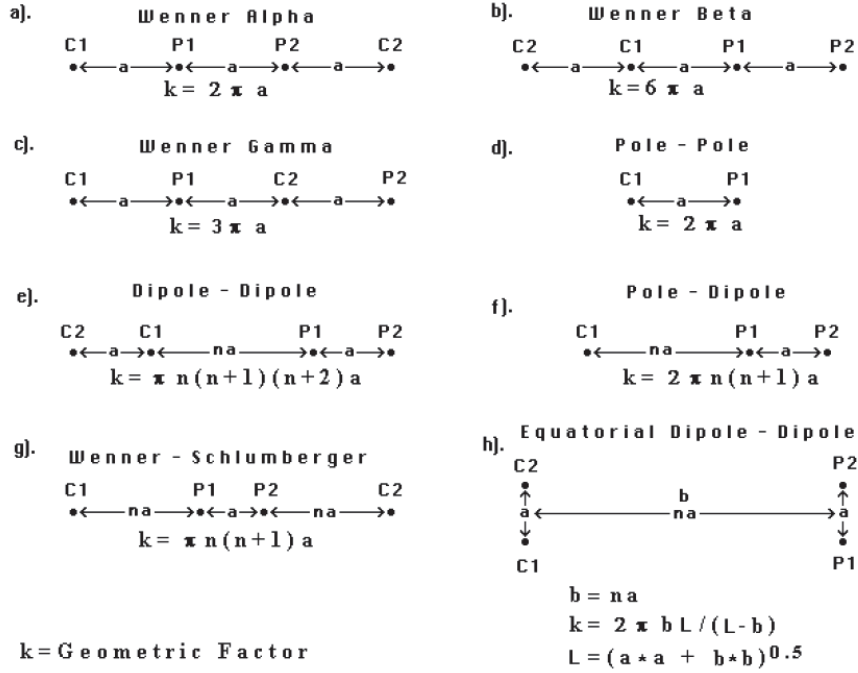


Figure 8: Illustration of different electrode configurations (Loke, 2016).

In Loke (2016) it is stated that the dipole-dipole array is sensitive to horizontal resistivity changes. This makes the array suitable for mapping of sedimentary layers, but it requires good ground contact. “The resistivity meter should have comparatively high sensitivity and very good noise rejection circuitry, and there should be good contact between the electrodes and the ground” (Loke, 2016). Equation 2.4 gives an example of the apparent resistivity, ρ_a , by use of a dipole-dipole configuration:

$$\rho_a = \pi a n(n+1)(n+2) \frac{\Delta V}{I} \quad (2.4)$$

where the distance between the pair of current electrodes and the pair of potential electrodes, a , is kept constant. n is the distance between current and potential electrodes (Sharma, 1997). This is a ratio (length/depth) which can be increased to increase investigation depth (Loke, 2016, p. 32).

The same principles count for waterborne ERT when a cable with electrodes is towed behind a boat (figure 9). The water above the sediments will be an additional layer in the resistivity data. Temperature and the amount of dissolved salts in the water will affect the resistivity of the water body. The ion activity in water will increase with increasing temperature, leading to lower resistivity. It is generally necessary to perform water conductivity measurements during a waterborne ERT survey.

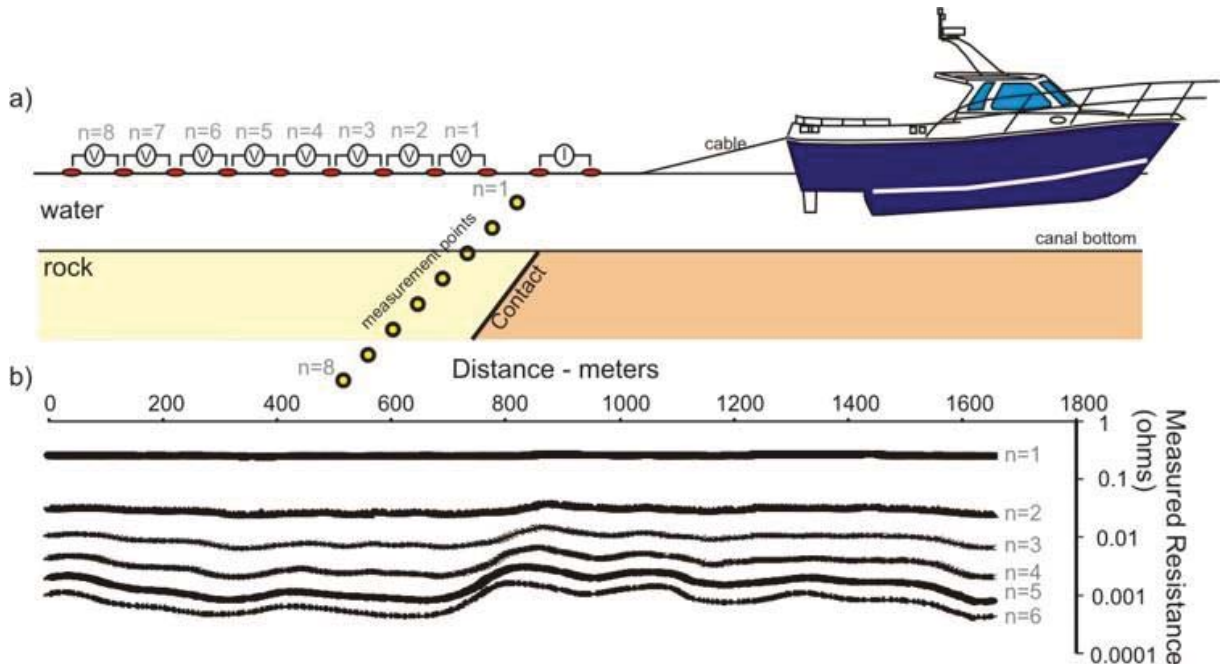


Figure 9: Sketch of waterborne ERT, showing the cable with electrodes towed behind a boat (a)) and measured resistance by depth (b)) (Rucker et al., 2011)

The measured resistivity values are used in the data programme RES2DINV, which makes a model of blocks with horizontal layers based on the measured values of resistivity. Vertical layers are added by the program, creating blocks (Loke, 2016, p. 2). An apparent resistivity (ρ_a) is calculated for each block, and gives an interpretation of the collected data:

$$\rho_a = k \times R \quad (2.5)$$

The geometric factor k depends on the electrode arrangement (Loke, 2016).

3.1.2 Advantages and limitations

Use of waterborne ERT as a method is described in literature, with focus on both collection and processing of data. One clear advantage of ERT is the range of the method, with the possibility of giving high-resolution data at the same time. Thousands of meters of data can be obtained during a relatively short time when the cable is towed behind a boat (Rucker et al., 2011). In e.g. Day-Lewis et al. (2006) up to 20 km of data is collected per day, at a speed of 4 knots (~7 km/h). For the best results, data should be collected in horizontal, straight lines. Drifting of the cable, due to currents, waves or wind could cause errors in data (Day-Lewis et al., 2006). It is also recommended to keep a low and steady pace. In this way stacking of measurements and errors from repeated data points can be avoided when processing the data. From literature it is recommended to compare ERT-data with other data for interpretation of results, e.g. compare resistivity values from the seabed and subsurface with maps, drill-core information or sonar-data (Dahlin et al., 2014; Epting et al., 2012).

3.1.3 ERT data collection and processing

Electrical resistivity tomography data were collected in the beginning of November 2017. The ERT measurements were carried out using a ‘SuperSting R8’ from Advanced Geosciences Inc. (AGI) (figure 10) with two marine cables with different electrode spacing. The cables were towed behind a small boat at the speed of approximately 2.16 to 2.70 knots (4-5 km/hour). A SuperSting marine WiFi-adaptor was used in combination with the SuperSting R8 to log the data to a tablet. The SuperSting R8 has a GPS which tracks the resistivity data from each profile. An additional GPS was also used, to have backup data. The marine cables were of two different lengths. The short cable had 11 electrodes with 6 m spacing, and the long cable had 12 m spacing. The graphite electrodes and the cable itself are grounded, to ensure that the current stays within the cable and is distributed to the electrodes. An additional GPS was used to have back up data, a ‘GeoXH 3.5’ from Trimble’s ‘Geoexplorer 6000 series’.

To avoid noise and interruption of the signal from the instrument to the marine cables, the Super Sting was insulated from the metal boat on a fiberglass floor. The batteries were insulated by keeping them in a plastic box. 30 cm long pieces of pipe insulation attached on the cable between every electrode prevented the cable from sinking, but kept the electrodes submerged in the water at the same time. The cable, GPS and WiFi-adaptor were all connected to the SuperSting R8 as the boat was towing the cable to collect data. The location of the boat was tracked on a tablet connected with a GPS, to ensure that the lines were as straight as possible when acquiring the ERT profiles.

A Solinst Levelogger Model 3001 (figure 10) was used to log water levels, temperatures and conductivity, σ . The instrument was towed behind the boat at approximately 1 meter depth. The data can be used to correct for resistivity values in the water above the layers of sediments (conductivity is the inverse of resistivity ($\sigma = 1/\rho$)). This gives data that are more precise and a possibility of better interpretation.



Figure 10: Show some equipment from the fieldwork. AGI SuperSting R8 (in picture A), the cable with electrodes towed behind the boat (B) and Solinst Levellogger (C).

RES2DINVx64, a 2D resistivity and inversion software (Loke, n.d) was used to process the ERT data. More information about the GeotomoSoftware can be found under ‘products’ at the webpage (Loke, n.d). A detailed manual under 'downloads' is available for free. Processing of the ERT data started by using AGI Super Sting Admin software to convert the raw data (stg-format). Challenges with missing and unstable GPS data collected by the SuperSting R8 GPS, made it necessary to reference the ERT data files with the external GPS data. Because of distances of several meters between the GPS and the first electrode on the ERT cable, some

corrections were made based on the positions and distances between the GPS in the boat and the length to the first electrode of ERT cable. These distances were 12 meters for the short cable, and 33 meters for the long cable. The ERT data were converted from the raw data (stg-format) combined with the external GPS data to a file that can be read by RES2DINV (dat-format). The estimated position of where the data points are collected are based on the distance between the GPS in the boat and the first electrode on the ERT cable.

The first point of measurement in a stg-file (last electrode) was defined as the start of the respective profile (0 meters), which made all four electrodes (in meters) for the first point of measurements known. Time stamps for each point of measurements from the stg-file makes it possible to find the GPS location for each point of measurement. The second point of measurement is found by estimating the distance between the electrode position of the first and second point of measurements from the GPS data. When this is continued for all points of measurements in a file, a dat-file is made based on the position of electrodes and resistivity values. NGI provided a script doing this and the dat-files that could be imported to RES2DINV.

After importing a dat-file in RES2DINV, the file is inverted and give results showing the apparent resistivity values of a profile. Several settings can be changed and improved for each file before inversion (suggestions of improvements are provided by the program). The previously mentioned manual provides detailed processing steps. In the inversion window, RMS (Root of Mean of Squares) statistics gives an impression of the quality of the ERT data. RMS “displays the distribution of the percentage difference between the logarithms of the measured and calculated apparent resistivity values” (Loke, 2016, p.53). The RMS is a relationship of the fit between measured and calculated apparent resistivity values for each model block. With high RMS error, the fit between the measured and calculated apparent resistivity values is low. The RMS errors should be considered as a measurement of the reliability of the data. $RMS < 5\%$ is good, but $RMS > 20\%$ should be considered as unreliable (Bazin, 2018 (personal communication)).

3.2 Ground penetrating radar

3.2.1 Theoretical background

Ground penetrating radar is a geophysical method used to investigate the subsurface. It is suitable for detecting buried objects like archaeological targets or old pipe lines, contaminations, the water table or geological structures (Schwartz & Zhang, 2003). GPR is a method based on electromagnetic wave reflection. A pulse is transmitted to the ground, and the reflected signal can be used to interpret the ground structures (figure 11). Changes and differences in conductivity and dielectric constants in layers or structures will cause reflection of the electromagnetic waves.

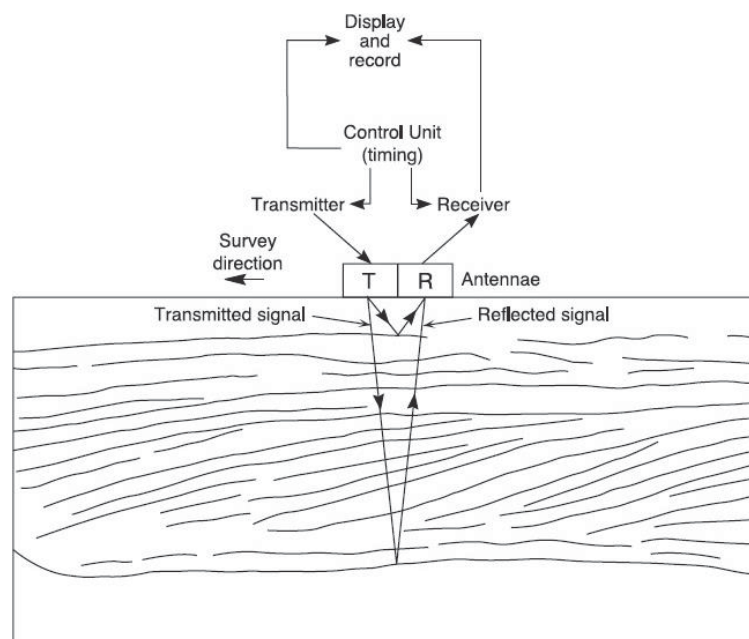


Figure 11: Principles of ground penetrating radar (Neal, 2004, fig. 3a)

Penetration depth is dependent on the frequency of the signal transmitted, dielectric constants and conductivity of the sediments, soils or bedrock. Frequencies used in the transmitted signals from the GPR are usually values of 10 – 1000 MHz (megahertz). The lower the frequency, the higher is the penetration depth. High frequencies on the other hand will give lower penetration depth but better resolution and more detailed images of the subsurface. The time (measured in nanoseconds, ns) it takes from when an electromagnetic signal is transmitted until the reflected signal is received, is recorded. Because the signal is reflected, it has a two-way travel time (Sharma, 1997).

The composition of sediments and saturation of water is important for the penetration depth.

The penetration depth of a GPR is roughly estimated by:

$$d = \frac{35}{\sigma} \quad (2.6)$$

where electrical conductivity, σ , is measured in mS/m (Schwartz & Zhang, 2003). The penetration depth will decrease with an increase in conductivity, e.g. clay or sediments saturated with brackish groundwater. It is also dependent on the velocity of the EM waves and the dielectric values in the soils and sediments in the subsurface. Equation 2.7 below is therefore more precise:

$$d = \frac{VT}{2} \quad (2.7)$$

where t is the two-way travel time (ns) and V is the average electromagnetic wave velocity (m/ns) (Beres & Haeni, 1991). V is dependent on the:

$$V = \frac{c}{\epsilon^{0.5}} \quad (2.8)$$

where c is the speed of light ($\sim 2.99 \times 10^8$ m/s) and ϵ is the relative dielectric permittivity (dimensionless). The dielectric constants will increase with increasing ion activity and water content/water saturation of the soils and sediments. Some dielectric constants and propagation velocities are presented in table 2. Typical maximum penetration depths are approximately 60 m for sand and gravel, 15 - 25 m for fresh water, 2 - 4 for clay and 75 - 300 m for bedrock (Mauringer et al., 1996).

Table 2: Dielectric constant and propagation velocity properties of some selected materials. (Modified version of table 8.1, Sharma (1997)).

Material	Dielectric constant, ϵ_r	Propagation velocity, V (m/ns)
Dry sand/gravel	4-10	0.15-0.09
Wet sand/gravel	10-20	0.09-0.07
Dry clay/silt	3-6	0.17-0.12
Wet clay/silt	7-40	0.11-0.05
Fresh water	81	0.03
Air	1	0.3

Interpretation of GPR data requires recognition of typical reflection patterns, to easier understand structures and layers or transitions of sediments in the subsurface. The reflection configurations and suggested interpretation of the different reflections in figure 12 can be helpful in combination with e.g. quaternary maps or general knowledge about geomorphology.

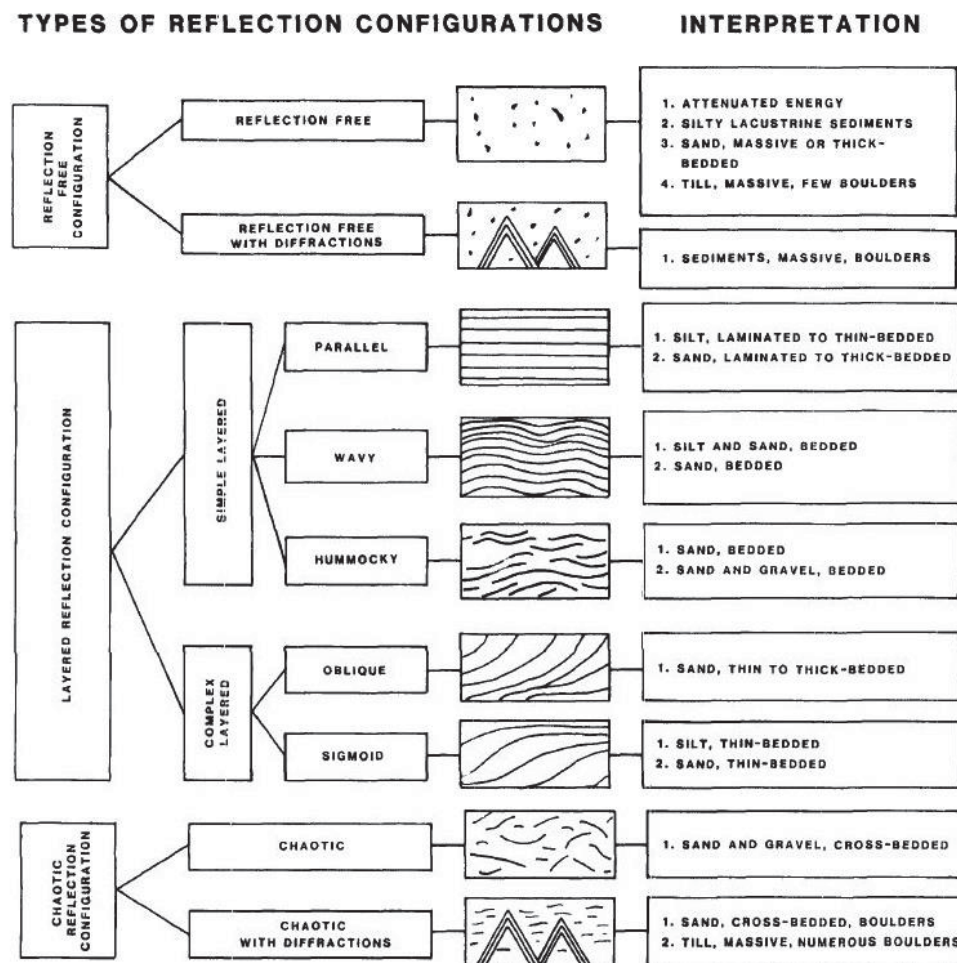


Figure 12: Interpretations of GPR reflections (Beres & Haeni, 1991, figure 3).

GPR data sets with layers of strong reflections can indicate high conductivity, which will lead the electromagnetic signal poorly through the underlying structures. High amounts of clay, saltwater intrusions or brackish groundwater could cause attenuation of the radar signal, giving very low penetration depths (Beres & Haeni, 1991).

3.2.2 Advantages and limitations

GPR is suitable for mapping and investigating vulnerable sites. The GPR can be placed on a cart with wheels, which makes it practical to handle. It is relatively light and leave barely any marks in the terrain, which makes the method suitable for use in places where motorized vehicles do not have access. The GPR can give high-resolution images of the subsurface and it is relatively cheap, and the data can be processed and give results consecutively. Different frequency of antennas will give data of different resolution and depth. Antennas with low frequencies will give a signal that can penetrate deep in resistive sediments, e.g. more than ten meters in dry sand and gravel (Beres & Haeni, 1991; Bristow & Jol, 2003). Higher frequencies will not penetrate as deep but give higher resolution and more detailed data, making it possible to characterize sediments (Vandenberghe & van Overmeeren, 1999). The penetration depth in conductive soils, e.g. clay, is limited (Di Prinzio et al., 2010).

3.2.3 GPR data collection and processing

Ground penetrating radar data were collected in the middle of April 2018, along seven profiles along Numedalslågen in Larvik. Two profiles were collected from Hvittensand and one at Skreppestad at the SE side of the river. On the N/NE side of Numedalslågen, one profile was sampled at Revet, one along the riverbank next to Elveveien and one profile at Orøya. The samples at Revet and Hvittensand are on each side of the delta. Some snow was still left at Orøya. Anthropogenic material, fillings and disturbance are expected to affect the profiles at all locations. Pictures from Hvittensand in figure 13.



Figure 13: Picture of Hvittensand taken from the spit (A), the beach and river mouth (left side) seen from the SW (B) and Hvittensand seen from Revet (C).

The GPR is a pulseEKKO PRO on a SmartCart from Sensors & Software Inc. (figure 14). The SmartCart has wheels, which makes it easy to use the GPR. The GPR was used with 50MHz antennas. The transmitting antenna sends a pulse into the ground, which is reflected to the receiving antenna. The preliminary results were monitored on the digital video logger, DVL. A Topcon HiPer II GNSS (Global Navigation Satellite System) receiver is tracking the position and approximately height above the sea level. In addition, there is an odometer recording the length of the profiles. The white box on the handle of the SmartCart has a button that can be pushed to add marks in the datasets. This function is useful to get the exact position of objects that are highly likely to disturb the data sets, e.g. lampposts or the beginning and end of snow covers or concrete pavements etc.

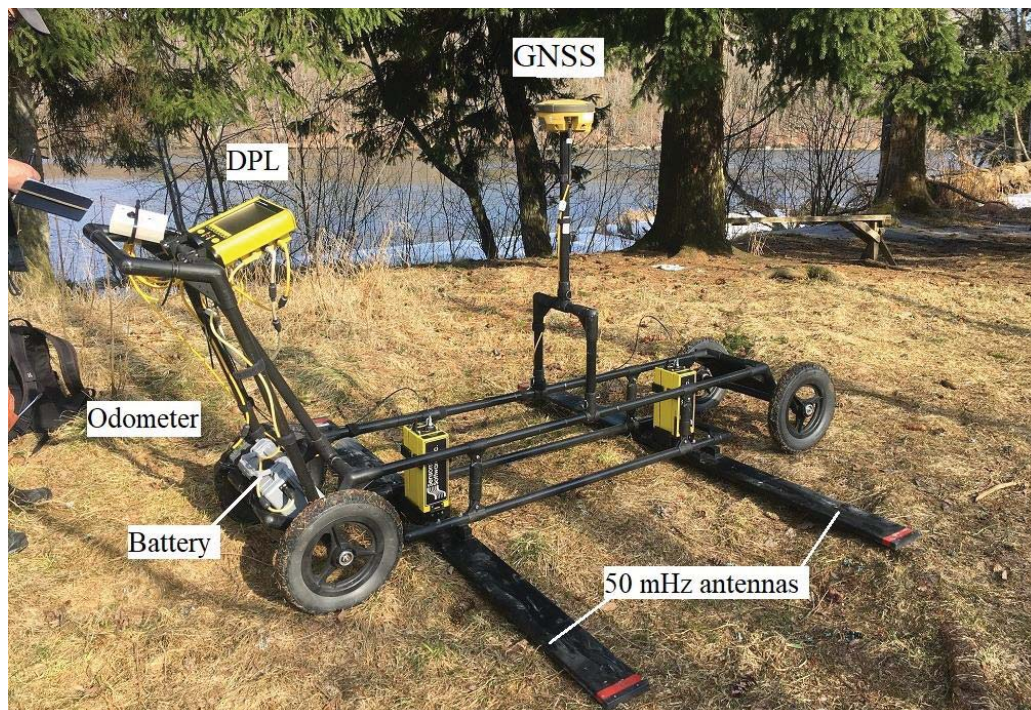


Figure 14: The GPR PulseEKKO PRO and SmartCart from Sensors & Software.

The GPR data was processed by using the PulseEKKO processing programme. Two user's guides from Sensors and Software Inc. were used, "EKKO_project" and "EKKO_Project LineView & Interpretations Modules" (Sensors and Software Inc., 2016; Sensors and Software Inc., 2017). The EKKO_Project User Guide provides information about the program, and how to edit, process and interpret GPR data. The separate manual Project LineView was used for processing of the profiles. In addition to using PulseEKKO for processing of the data, new figures of the interpretations were made by using Inkscape, a free vector graphics editor.

4. Results

4.1 ERT results

From the 49 lines collected in Larvik, a total of six profiles (labelled in yellow in figure 15) are presented here, in addition to figures from processing of the data. The ERT lines were collected either in NE – SW direction parallel with the river flow (e.g. profile p1, p3, p6 and p9) or in NW – SE direction transverse of the river flow (e.g. profile s1 and s4). These six profiles are presented with the same scale for resistivity, ranging from 0.02 to 63 Ωm , and the colour scale is consistent.

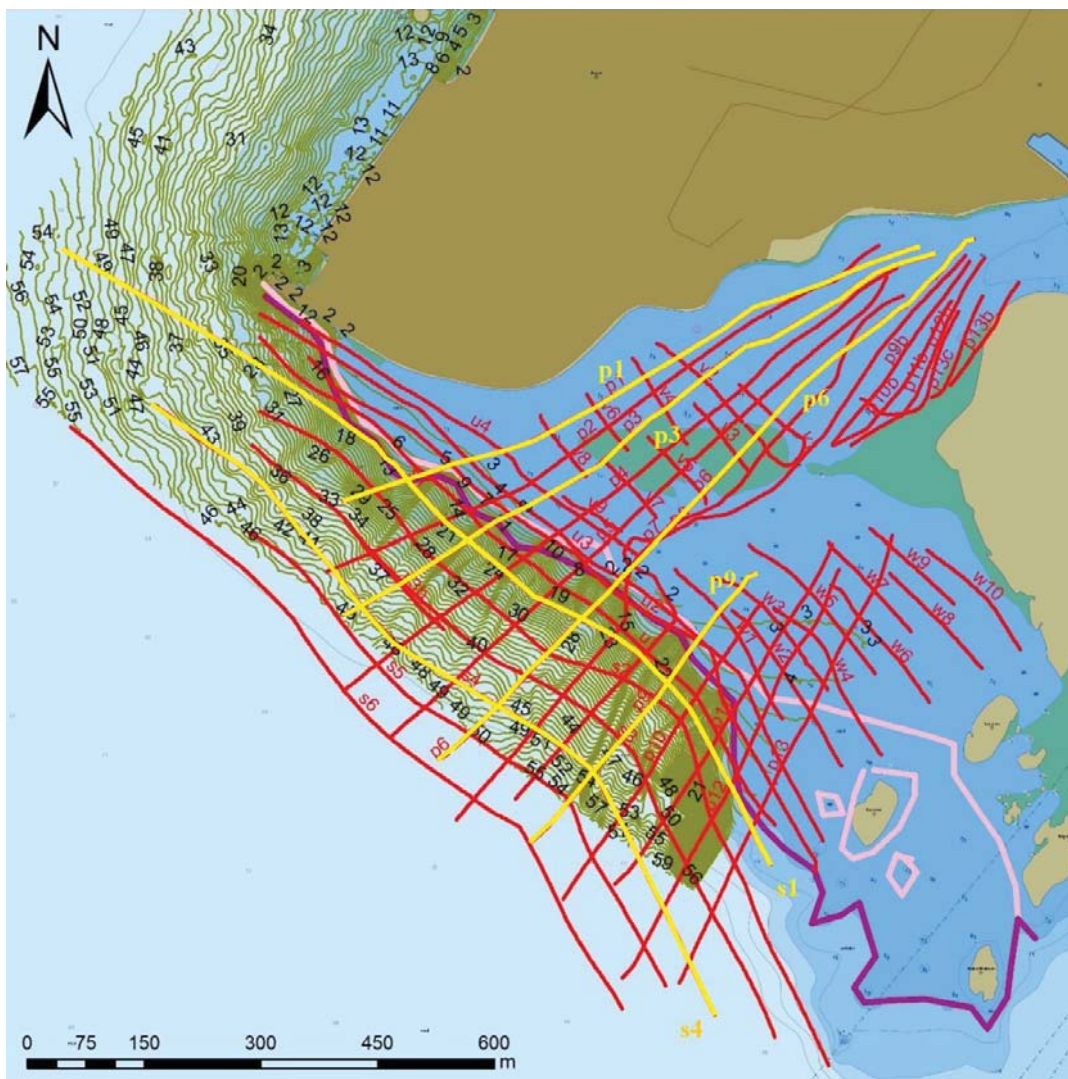


Figure 15: The delta area between Revet and Hvittensand in Larvik. Lines with labelling in red are the collected ERT data. The green lines are contour lines with depths in black numbers. The pink and purple line divides sea shallower than 5 and 10 meters respectively from the fjord.

Data collected with the Levellogger (figure 16) were included in the ERT data. The measurements are collected at approximately 1 meter depth but show high variations in conductivity values (number by each data point in figure 16). The conductivity measurements range with values from 0 to 36 784 $\mu\text{S}/\text{cm}$. The measurements seems random, but if the conductivity measurements of 0 $\mu\text{S}/\text{cm}$ are ignored, a trend of conductivity values above 1000 $\mu\text{S}/\text{cm}$ are found in the area SE of the Spit and Hvittensand, and values lower than approximately 300 $\mu\text{S}/\text{cm}$ are found between Revet and Hvittensand. Towards the fjord SW of Revet the values increases. The temperature values are ranging between 3.5 and 8.7 $^{\circ}\text{C}$. Between Revet and Hvittensand, close to Hvittensand in NE values above 6 $^{\circ}\text{C}$, before the measured temperatures decreases towards the fjord. Some higher temperatures (approximately 5.5 $^{\circ}\text{C}$) are observed in the points NE of Revet. SE of Hvittensand and the spit, most of the measured temperature points are between 6 – 8.7 $^{\circ}\text{C}$. The highest measured conductivity value from the survey, 36784 micro-Siemens/cm (equals 0.27 Ωm) was chosen as the starting resistivity of the waterbody in RES2DINV.

Figure 18-22 gives an insight in challenges with processing of ERT data. In figure 17, bad data points among all the measured data points are differing from most of the resistivity values. Some of them are pointed out. These points could be removed, but in figure 18 it is impossible to determine which data points that are ‘reliable’ and which ones that are not. Another problem with removing data points are displayed in figure 19. The number of measured data points are very few, compared to the number of model blocks presented by the modelling program RES2DINV. Too few data point does not increase the confidence in the data. In this case it does not make much of a difference, as the quality of the processed ERT profiles in general is quite low.

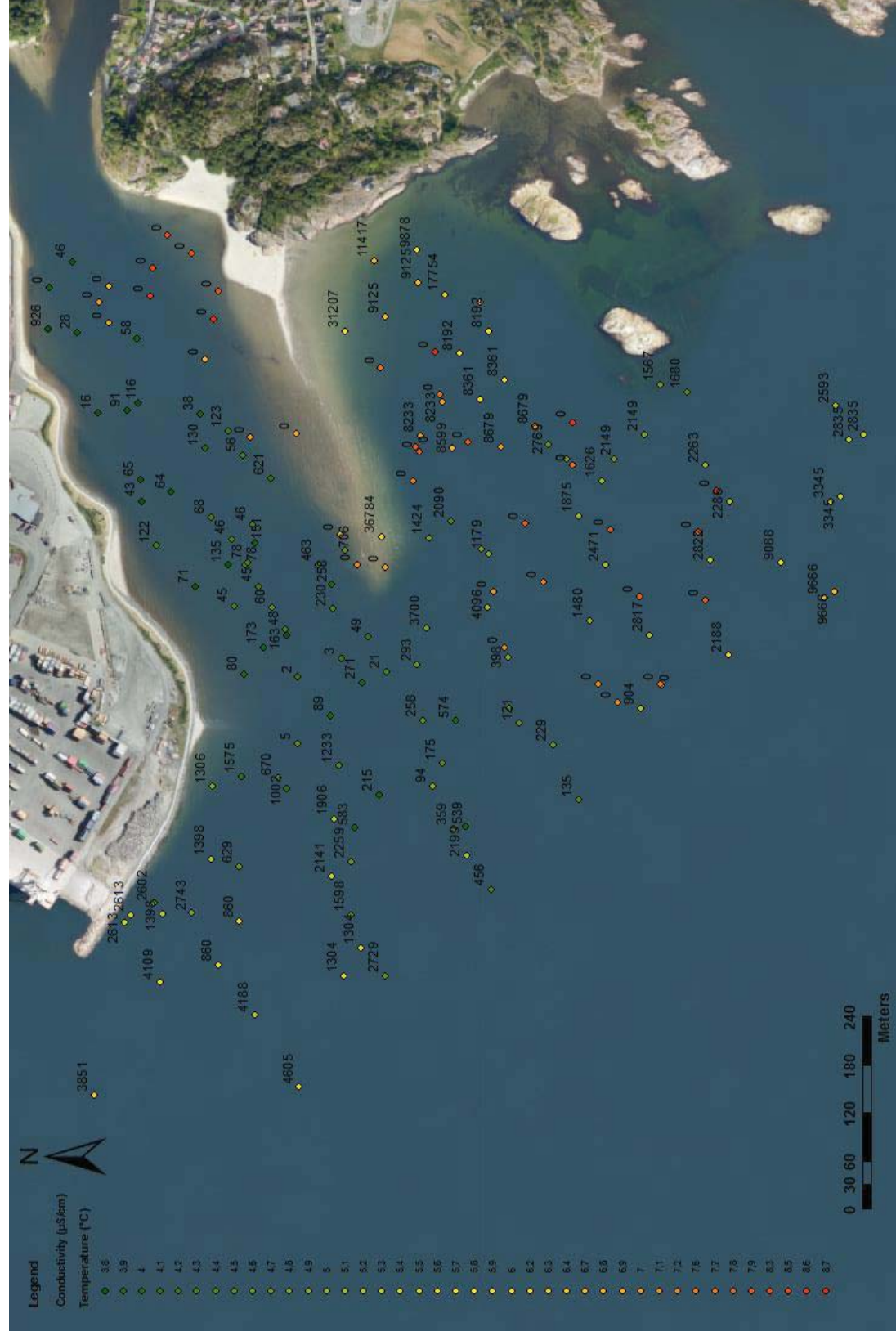


Figure 16: Temperatures ($^{\circ}\text{C}$) in colour and conductivities ($\mu\text{S/cm}$) labelled with numbers for each data point. (Map from Kartverkets WMS (GeoNorge, n.d)

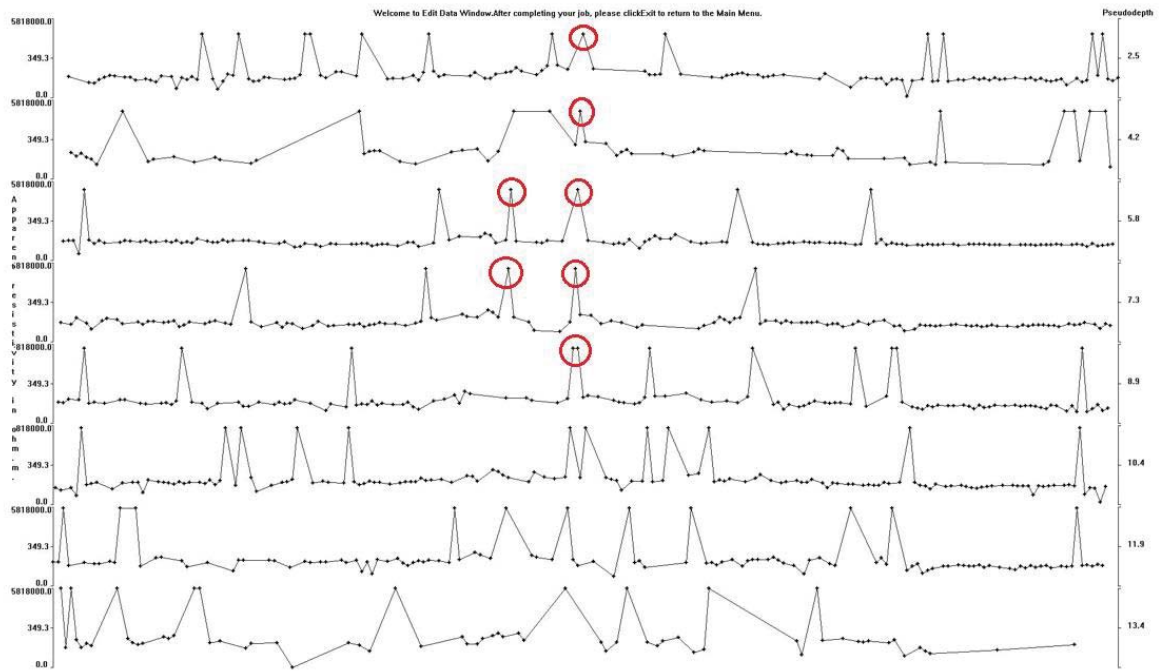


Figure 17: ERT data points for profile S1 from an editing window in RES2DINV. Apparent resistivity values in Ωm on the left y-axis compared to the pseudo depths on the right y-axis. Several data points are sticking out as spikes compared to the rest (some of them are marked in red).

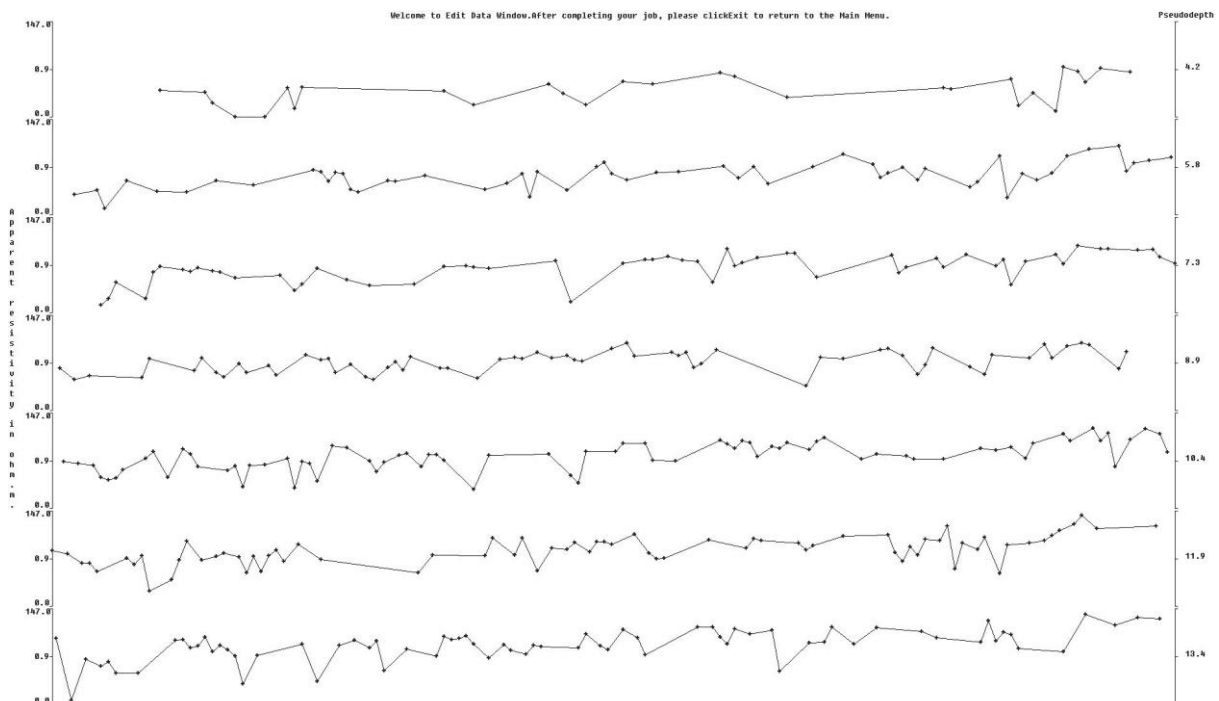


Figure 18: ERT data points for profile p3. Apparent resistivity values in Ωm on the left y-axis, pseudodepths on the right y-axis. There are quite few datapoints and it is difficult to determine which data points are good and which are bad.

During processing of the ERT data, the relationship between model blocks and data points are pointed out with a bad fit (figure 19). RES2DINV makes model blocks, and in figure 19 this is presented with the topography of the delta top, based on bathymetry data. The collected data points are displayed as X's, and from the figure it is clear that compared to the model blocks it is too few points and in addition the signal of the ERT does not penetrate deep enough through the water. The current lines between current and potential electrodes do not reach the sediment layers. Figure 19 show a large number of model blocks and a low number of data points.

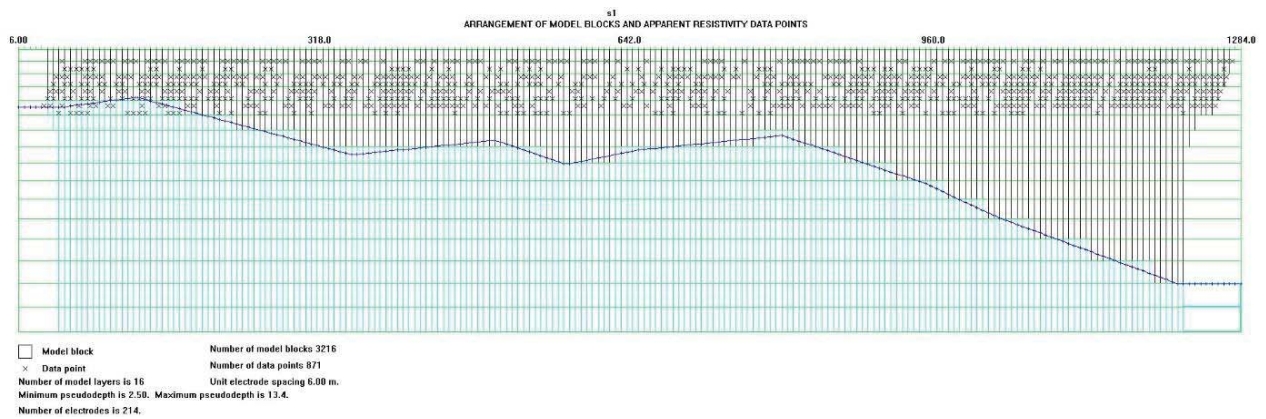


Figure 19: ERT profile s1 showing a comparison of the collected measurements with 3216 model blocks and 871 data points. The dark blue line presents the bathymetry, with the delta beneath displayed as light blue blocks.

The RMS statistics (figure 20 and 21) gives an impression of the apparent resistivity error in percent as histograms (a) and as the fit between calculated apparent resistivity on the y-axis and measured apparent resistivity on the x-axis (b). The plot in figure 20 are the original for profile S1. In figure 21, the data are trimmed, so that the points that exceeds 100% error is removed. The fit of the points should optimally follow the linear curve. In 20 b the points are gathered in the centre of the plot as a cloud. After trimming the data (21 b), the points are more evenly spread along the linear curve.

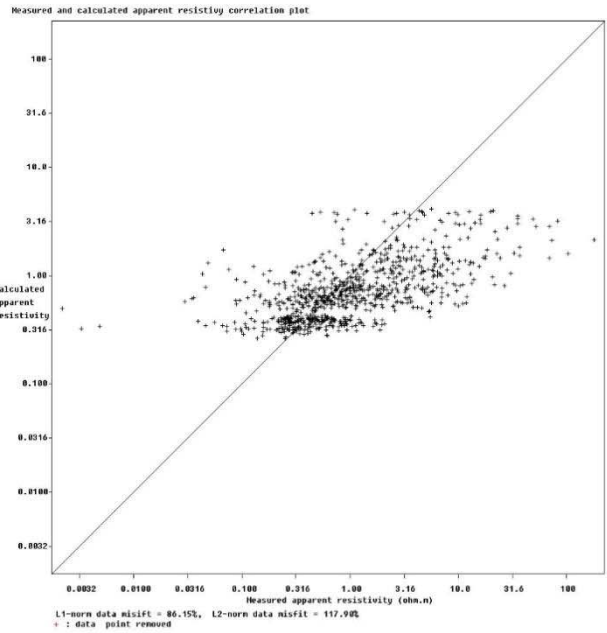
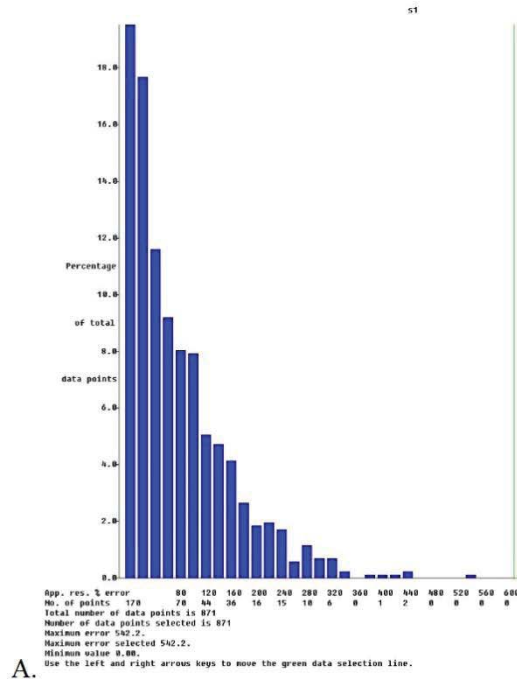


Figure 20: ERT data points from profile S1 displayed as histograms in A., based on number of measured points with specific RMS errors. Increasing error percentage from left to right. The data are plotted in B., comparing calculated and measured apparent resistivity values.

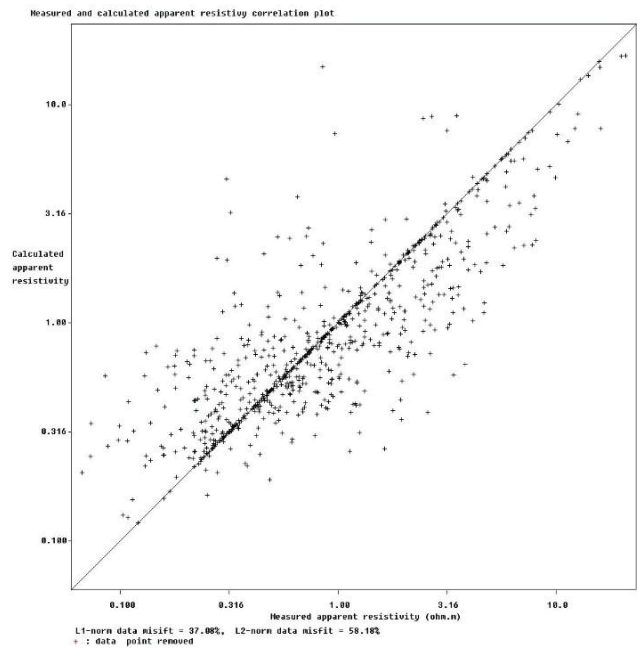
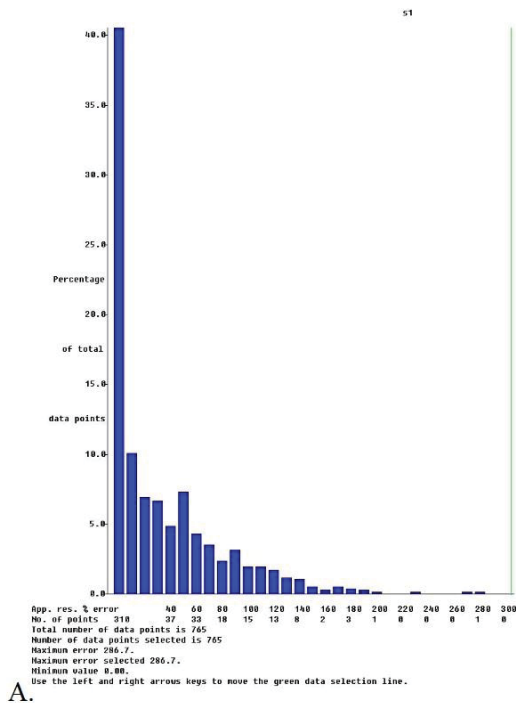


Figure 21: ERT data points for profile S1. The data are trimmed, histograms with RMS above 100% are removed in A., and the fit of the plot between calculated and measured apparent resistivity are spread more evenly along the linear line in B.

The ERT lines p1, p2, p6 and p9 between Revet and Hvittensand are presented in figure 22-27, orientated in parallel direction with the water flow. The resistivity values in the profiles are highest closest to the river mouth and decreasing in SW direction towards the fjord. The resistivity values on the delta slope are low and varying both in the upper sections that represent the water body and the lower parts that represents the delta, roughly between 0.6 and 6 Ωm . In addition is the resistivity values highly varying and changing between the depths of approximately 1 and 12 meters. Resistivity values higher than 20 Ωm are found in the river segments of roughly one third of the profiles p1, p3 and p6 (figure 22-24). Conductivity values from line p1 and p3 in figure 16 are plotted on the respective profiles in figure 22 and 23. The conductivities are varying just as the resistivity values. With some exceptions from the conductivity values toward the NE ends of the profiles, the conductivities seem to decrease from SW towards NE, whereas the resistivity values increases. P9 is a shorter profile of less than 500 meters (figure 25). The profile is short and collected in NW – SE direction south of the spit at Hvittensand (figure 15). The resistivity values are low and in the delta gradient, disruption of the signal does not give a continuous gradient. The resistivity values range from 0.02 to a little less than 0.6 Ωm . All the profiles have an RMS higher than 93 %, profile p1 after four iterations and p3, p6 and p9 after seven iterations.

The profiles transverse of the direction of the river are s1 and s4. Profile s1 (figure 26) show some horizontal differences in resistivity, unlike the rest of the profiles. The water layer in the top section of the profile (0 to approximately 8 meters depth) have resistivity values that mainly ranges between 6 and 20 Ωm between 450 and 870 meters (horizontal direction). These are higher than the surrounding resistivity values of the water layer. From 12.3 – 33.4 meters depth in the left end of the profile, resistivity values of approximately 20 Ωm are present. Further down and further right of the area with a resistivity of 20 Ωm , the resistivity is decreasing to values less than 7 Ωm . From 924 to 1026 meters, below 25 meters depth, the resistivity values range from 20 to more than 63 Ωm . Profile S4 (figure 27) show lower resistivity values, between 0.02 and 2 Ωm . There is no logical pattern, with resistivity values lower than 0.2 Ωm in both the top and bottom of the profile, in addition to one square of higher resistivity (2 Ωm) in the middle of the profile between 1 and 25 meters depth. Both have RMS higher than 120 % after seven iterations.

The white lines drawn in profile p1, p3, p6, s1 and s4 are interpretations of approximately boundaries between the water body and the seabed, based on bathymetry data and resistivity changes in the profiles.

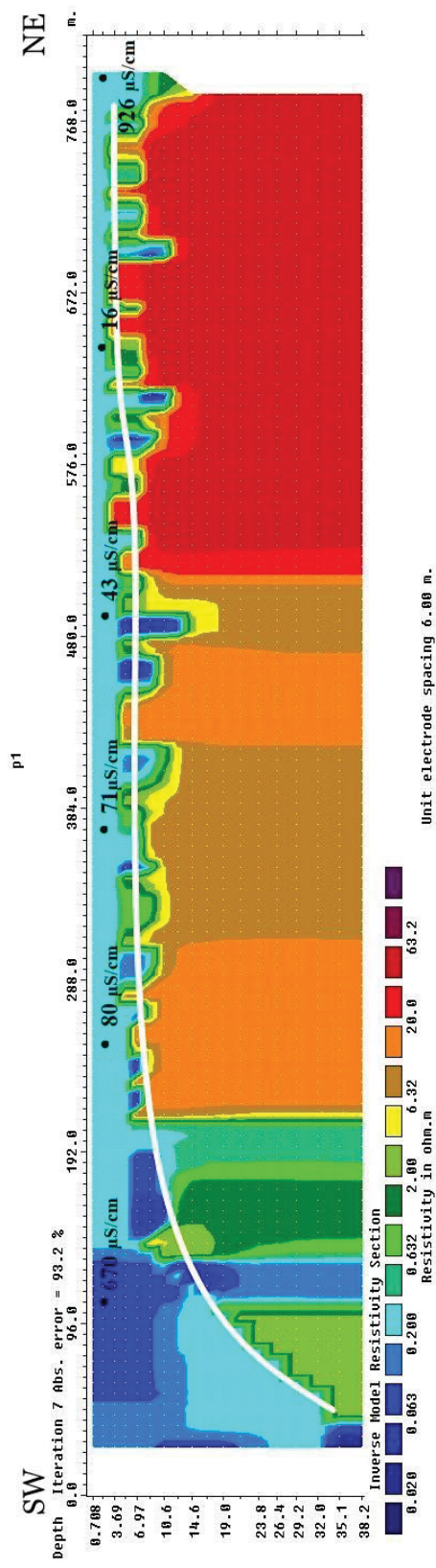


Figure 22: ERT profile p1. Several sections of different and repetitive resistivity are dominant from the SW to NE end of the profile. The unit electrode spacing is 6.00 meters. Length of the profile is shown on the x-axis, and the reach of depth for ERT measurements on y-axis. RMS error = 93.2 %

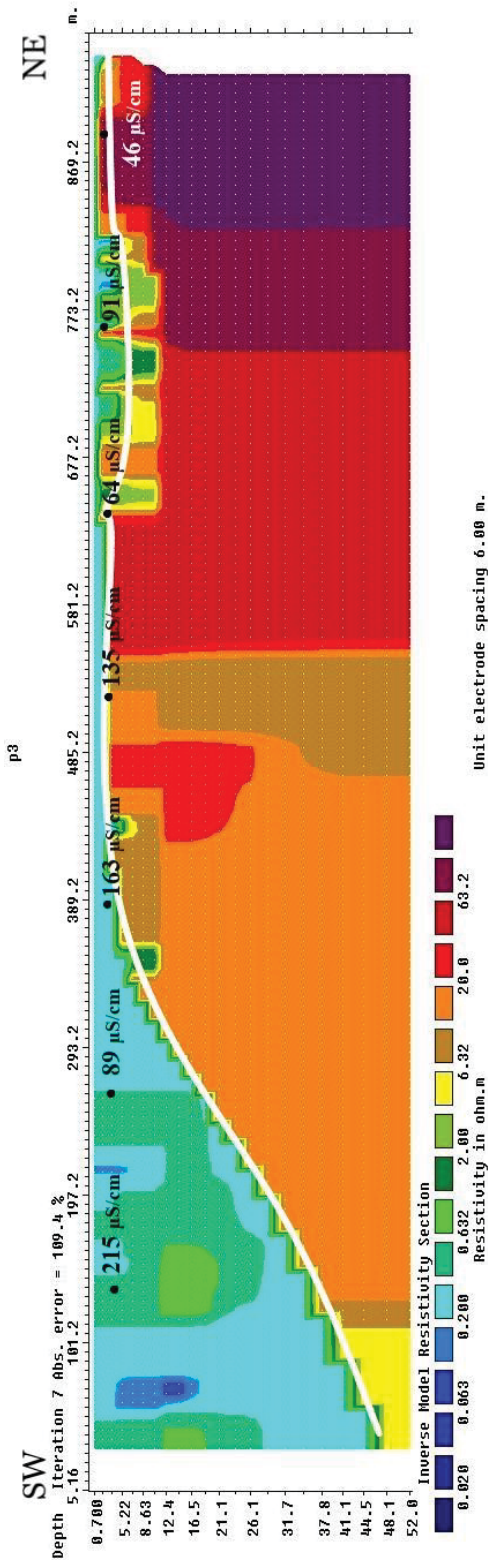


Figure 23: ERT profile p3 have an undisturbed gradient in the left end of the profile and increasing resistivity towards the right end of the profile. Between approximately 650 and 820 meters the resistivity values are varying between the surface and 12 meters depth. RMS error = 109.4 %

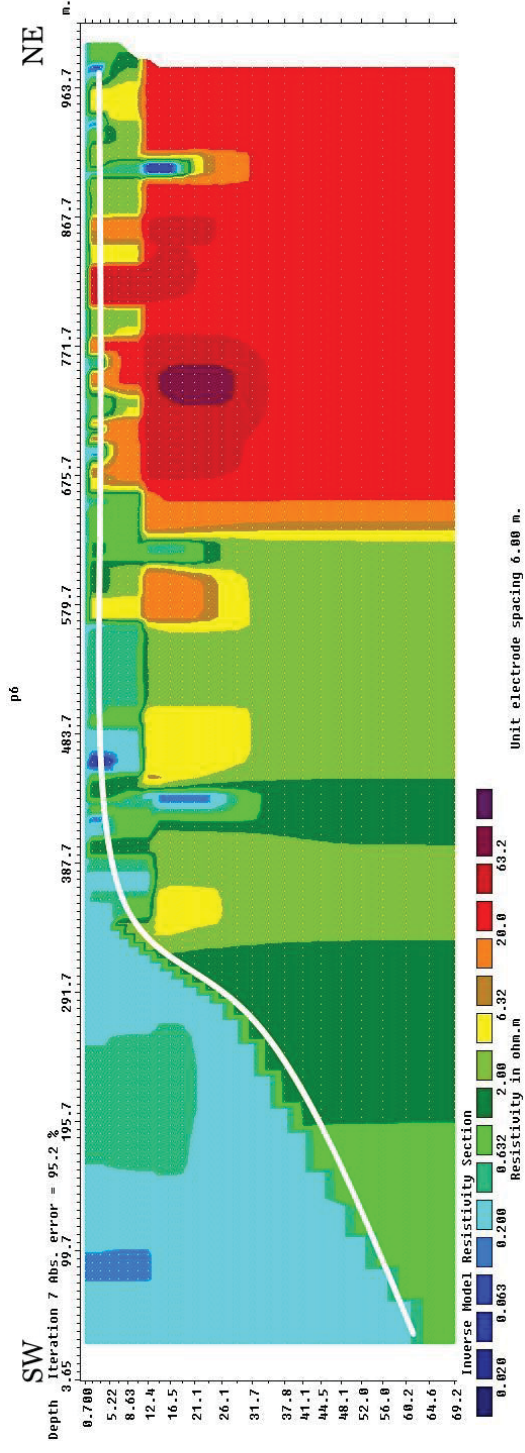


Figure 24: Resistivity mainly ranging from 2 to more than 20 Ω m in ERT profile P6. RMS error 95.2 %.

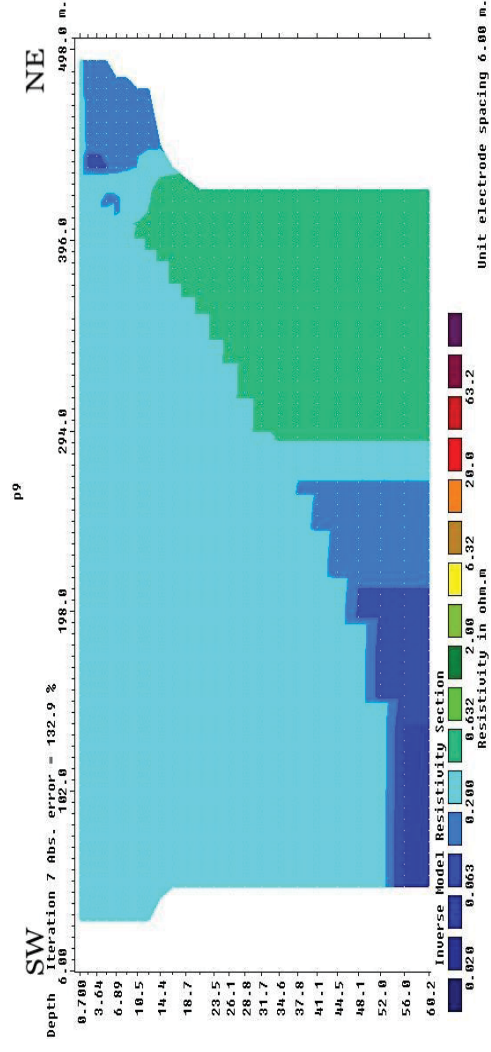


Figure 25: A short ERT profile (p9) collected SW of Hvittensand. The resistivity values are low, and the RMS error high with 132.9 %.

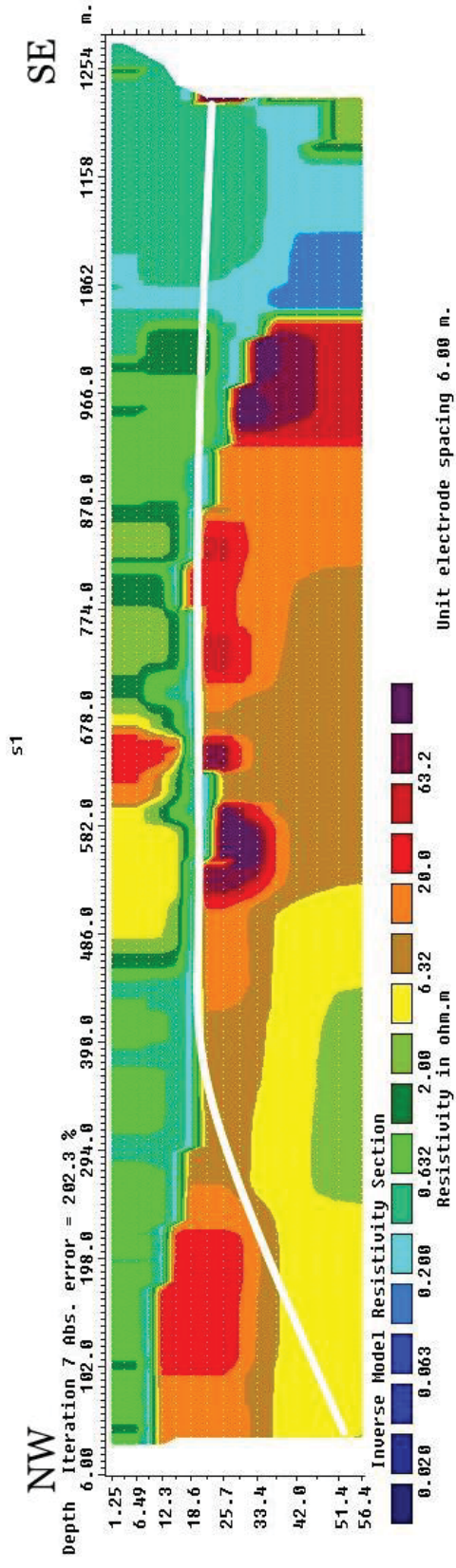


Figure 26: ERT profile S1, starting in NW at the left side of the profile, ending in SE. The white line is based on bathymetry data (figure 16). The RMS error is high with 202.3 %!

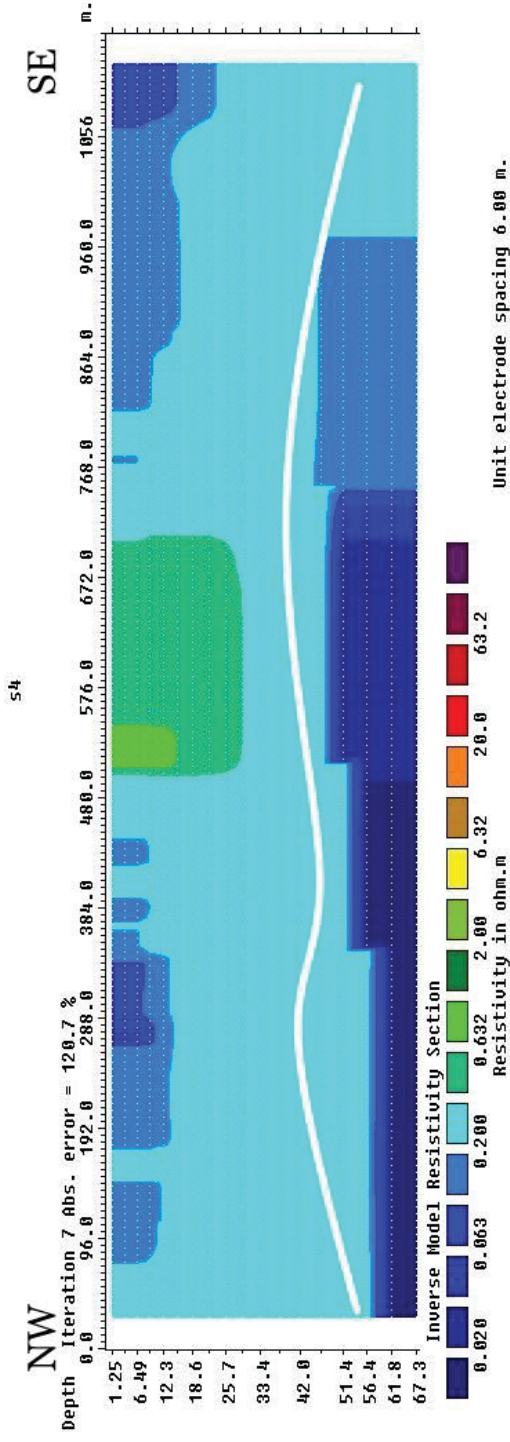


Figure 27: ERT profile S4 have low resistivity values. NW to SE directions from left to right. The white line is the approximately surface of the seabed, based on the interpretation of bathymetry data in figure 16. RMS error 120.7%.

4.2 GPR results

A total of seven GPR data were collected in five different locations (figure 28), table 3 gives a brief description of the location and possible disturbances. Here, only three profiles from Hvittensand (figure 29) are presented in figure 30-32. The remaining profiles, line 03 – line 06, are affected by disturbances, repetitions in signals and signal loss which gives poor results. These profiles are found in appendix D.

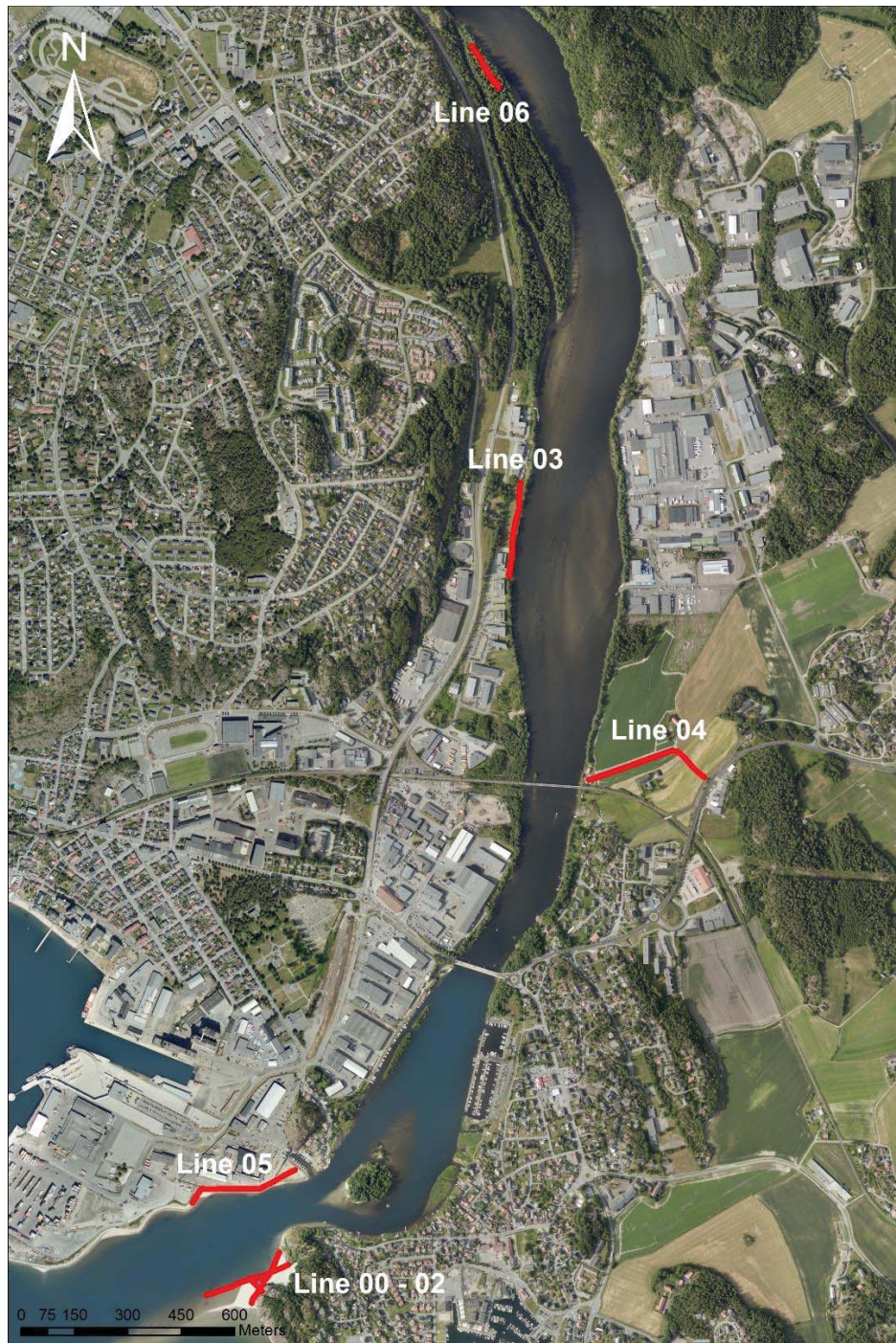


Figure 28: Locations of the collected GPR lines. (Map from Kartverkets WMS (GeoNorge, n.d))

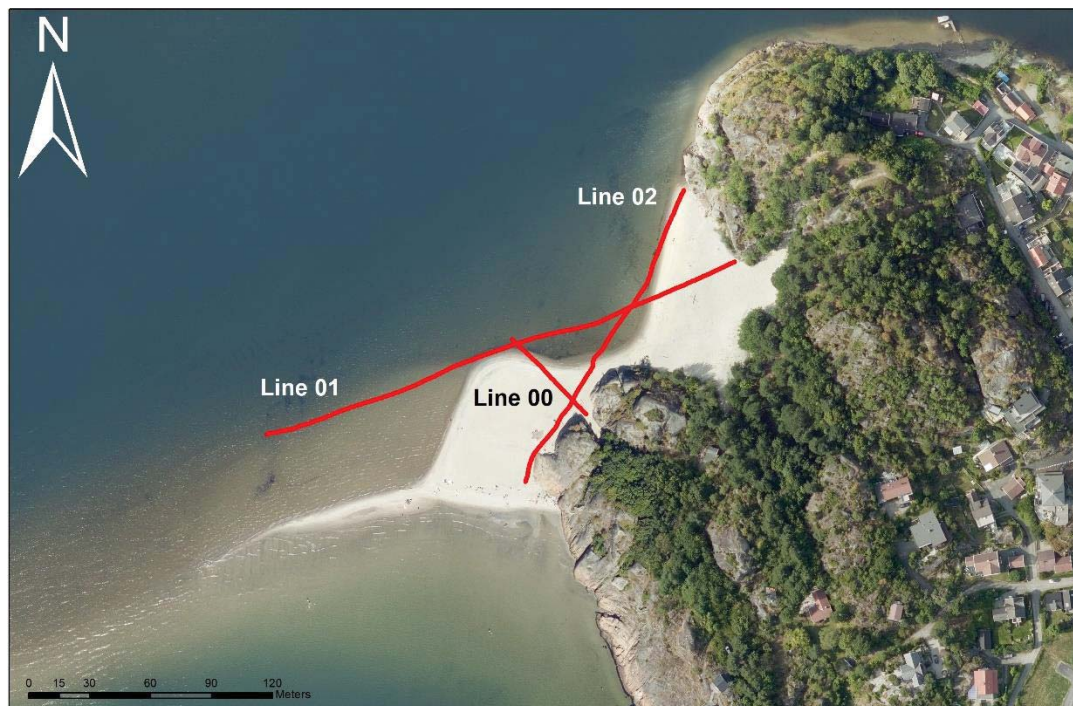












Figure 29: GPR lines from Hvittensand. (Map from Kartverkets WMS (GeoNorge, n.d))

Table 3: Locations, description and analysis of the GPR data sampling.

Line	Location	Direction	Descriptions	Possible disturbances
00	Hvittensand	SE → NW	Fluvial sand, natural. Outcrops of bedrock. Spit running into the water in the southern end.	0-2 m.a.s.l. Brackish/salt groundwater.
01		N → S		
02		S → N		
03	Elveveien	S → N	Flat area, approximately 1.5 m above the watertable of Numedalslågen. Grass, little other vegetation.	Anthropogenic disturbances. Buried well or similar.
04	Skreppestad	SE → N → SW	Road with gravel between two fields. Starting at the top of a hill/slope in the S end. End near the river.	Ditch on NE side. Pipes. Crossing one bridge.
05	Revet	S → N	Road of gravel. Anthropogenic filler. 1,5-2 m.a.s.l. Likely that brackish water infiltrating the groundwater.	Concrete in the S end. Several lampposts.
06	Orøya	N → S	1 m above the water table of the river Numedalslågen. Sandy deposits, some bedrock outcrop. Forest/vegetation.	Patches of snow on the path. Some trees.

The GPR profiles from Hvittensand (figure 30-32) are all presented in three different ways; the actual GPR profiles (A), a sketch with markings of the strongest reflections and most distinct structures and layers (B) and identification of GPR facies (C). The identification and interpretation of GPR facies are synthesised in table 4, and are based on reflections shown in figure 12 (Beres & Haeni, 1991). Some parts of the profiles are hard to interpret, as the reflections have poor signal and are not reliable. At depths where the signal does not penetrate (marked with a dotted line in GPR profiles), the interpretation is not completed.

Table 4: A comparison and interpretation of different GPR facies from Hvittensand. The interpretations are based on Beres and Haeni (1991).

Reflection pattern	Sketch	Colour	Description/interpretation
			Wavy 1. 'Silt and sand, bedded' 2. 'Sand, bedded'
			Hummocky 1. 'Sand, bedded' 2. 'Sand and gravel, bedded'
			Bedrock
			Reflection free

The profile of the short GPR line 00 from Hvittensand (figure 30) started by bedrock outcrops in the SE and ended towards the river to the NW (figure 29). The total distance of the profile is 46 meters. The top reflection is strong, and no interpretation was done below 5 meters towards the delta in the NW as the signal was lost at this depth. In the SE several structures between 5 and 20 meters depths are present. These reflections are partially interpreted as continuous and disrupted structures, interpreted to be wavy or hummocky layers.

GPR line 01 started in the N end of Hvittensand (figure 31) and ended at the spit running into the water in the south end of the beach (figure 29). At the northernmost part of the GPR profile, the repetitive reflections between approximately 3 and 20 meters depth are interpreted as bedrock. This corresponds with observed bedrock outcrops at Hvittensand. The reflections overlying the interpreted bedrock-facies, are wavy whereas hummocky layers are identified between 20 and 60 meters in the profile (figure 31). From approximately 60 meters to 220 meters, the profile is reflection free. This segment is collected close to the delta area, approximately 0.5 meter above the water in the delta. The strong top layer is a marker for the topography.

In GPR line 02 from Hvittensand (figure 32), a strong top layer reflection is present just as in figure 30 and 31. In addition to this, one strong reflection at 5 meters depth are found between 140-80 meters in the northern part of the profile. This is interpreted to be a bedrock surface, due to proximity to the bedrock outcrop at the beach (figure 29). Some vague reflections are surrounding this interpreted bedrock reflection. In the southern end, the reflection patterns interpreted as wavy layers dominate, with some possible hummocky structures between 15 and 35 meters (figure 32). A dotted line makes an approximately penetration depth of the profile. Below this line, the reliability of the data and interpretation is limited, especially in the northern end, as the data seems noisy and it is hard to estimate the gradient of the bedrock.

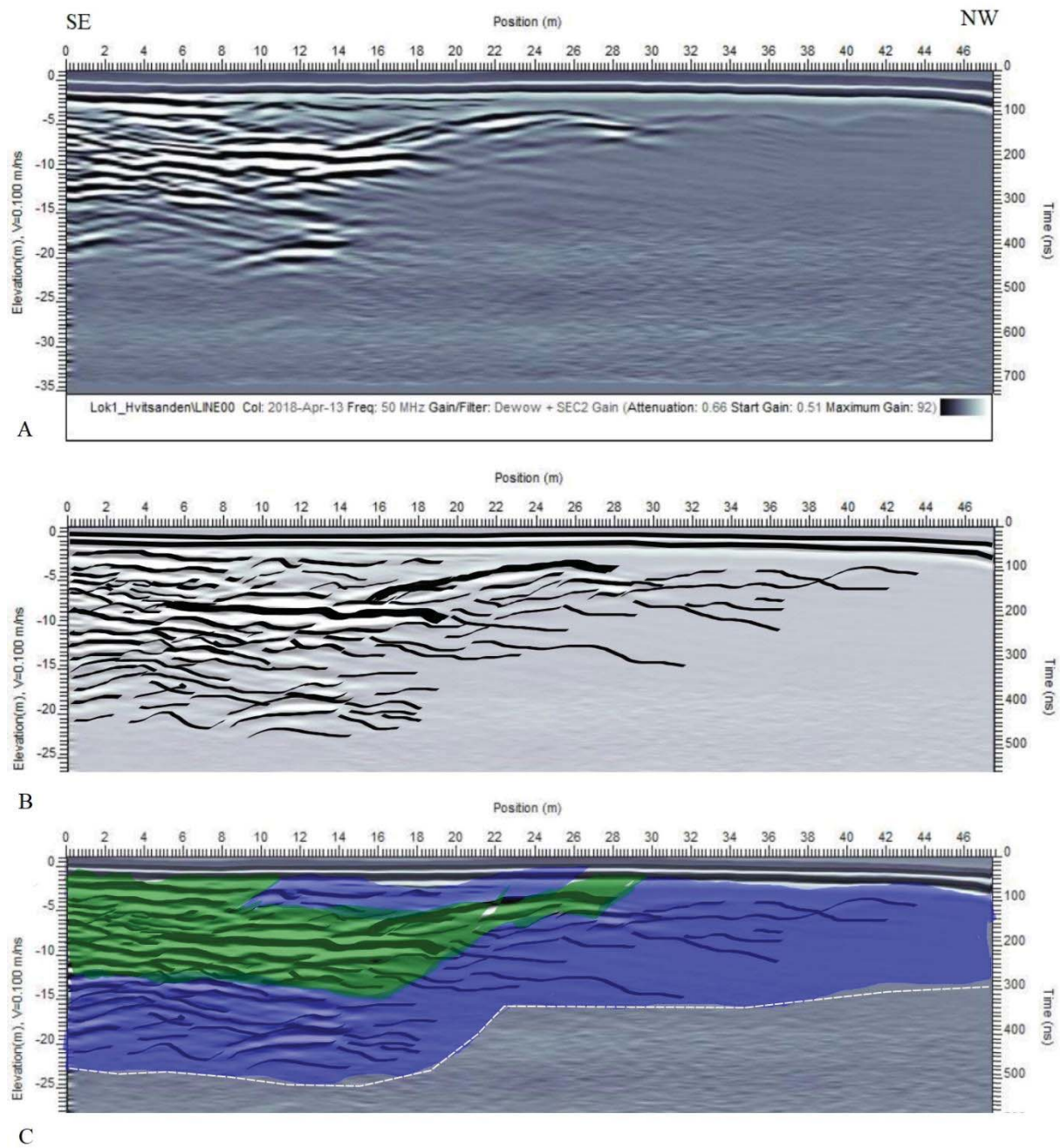


Figure 30: GPR line 00 from Hvittensand oriented SE to NW (A), with an interpretation of the strongest GPR reflections (B) and identified GPR facies (C). For legend, see table 4. Elevation in meters on the left y-axis.

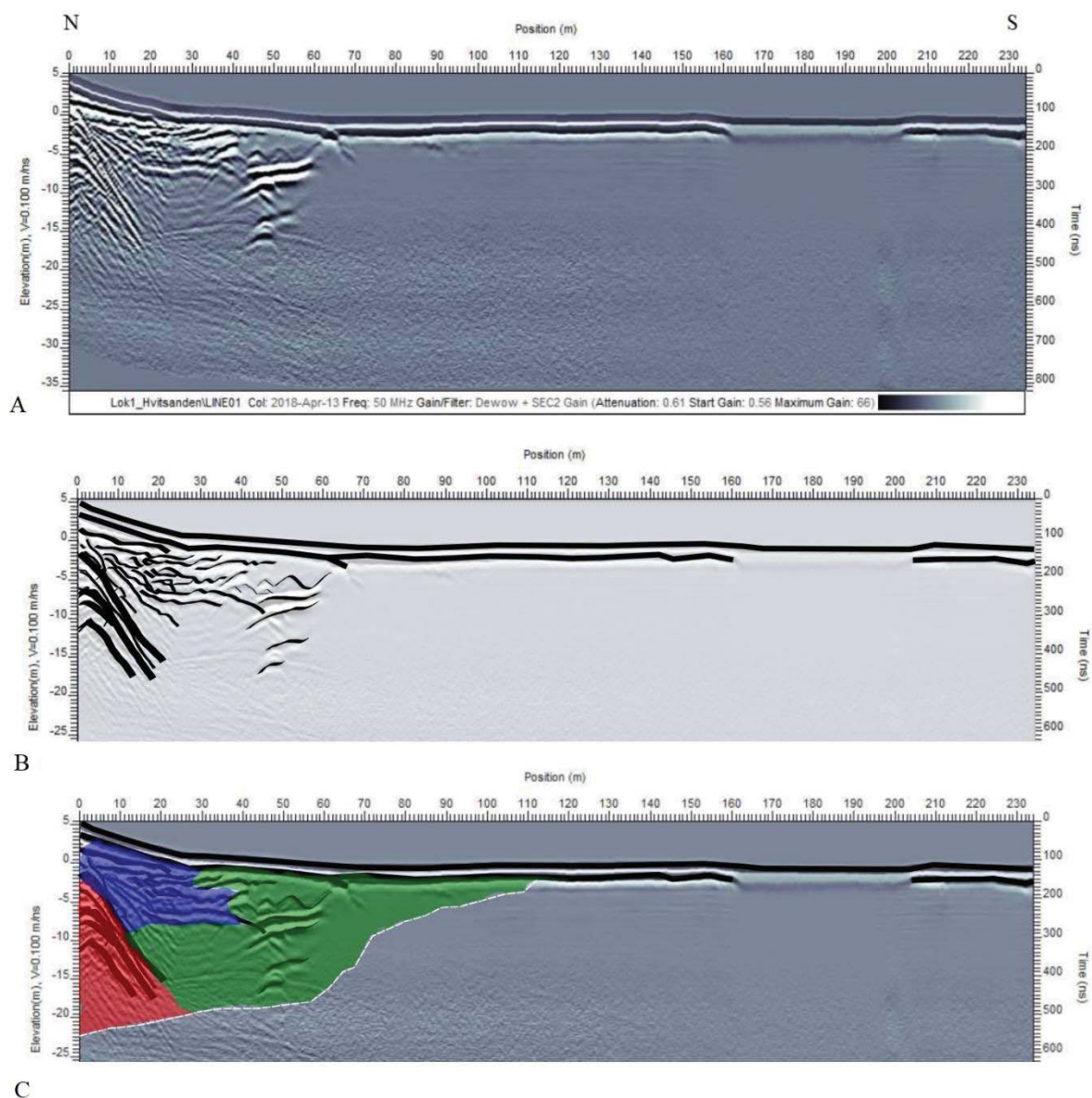


Figure 31: GPR line 01 from Hvittensand oriented N to S (A), with an interpretation of the strongest GPR reflections (B) and identified GPR facies (C). For legend, see table 4. Elevation in meters on the left y-axis.

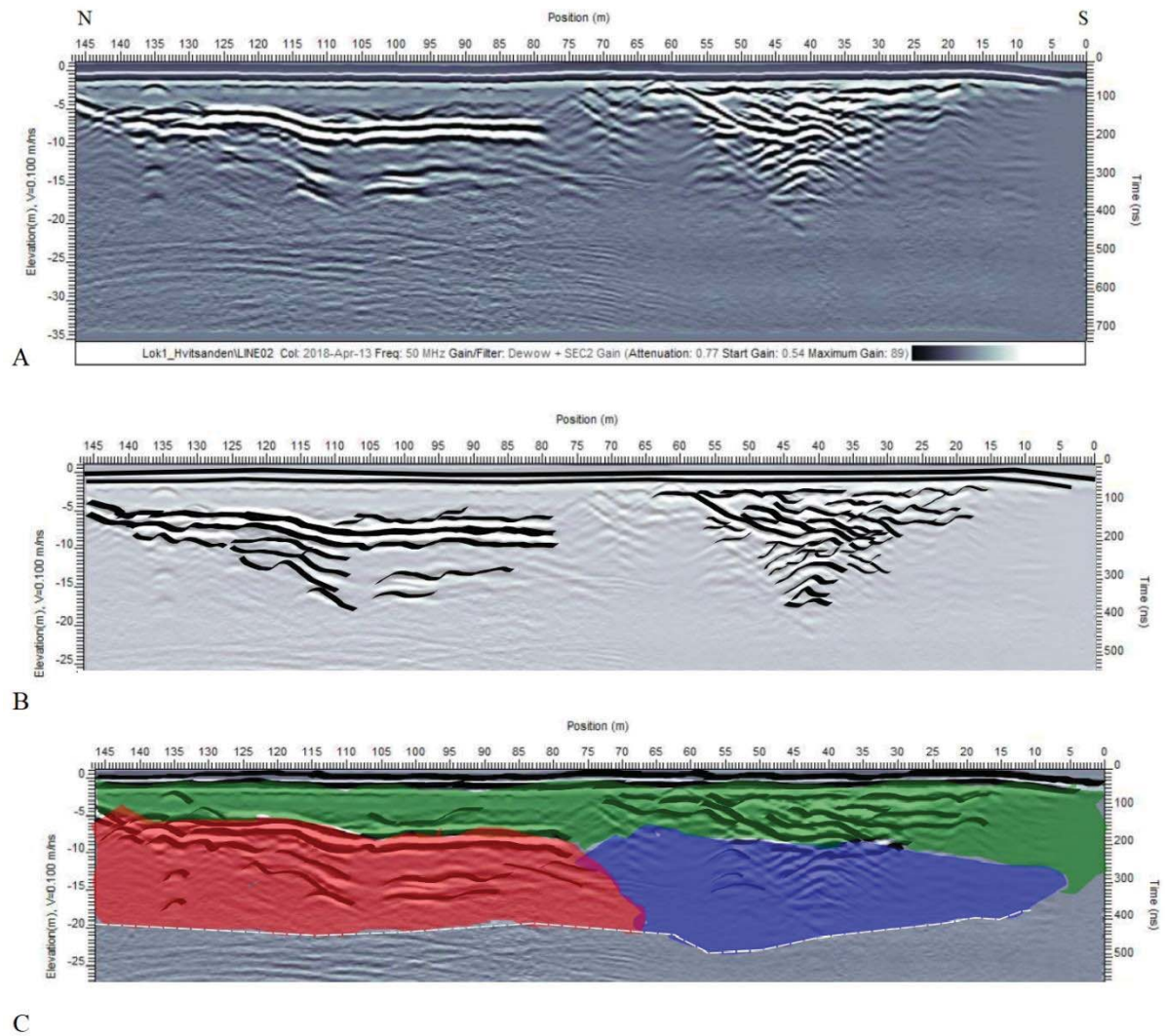


Fig 32: GPR line 02 from Hvittensand oriented N to S (A), with an interpretation of the strongest GPR reflections (B) and identified GPR facies (C). For legend, see table 4. Elevation in meters on the left y-axis.

5. Discussion

5.1 Discussion of ERT data

More than 30 lines of ERT data were collected, and six profiles were chosen for further interpretation. Processing of the ERT data in figure 22-27 included several adjustments. The quality of the ERT data is a result of challenging weather conditions with wind and waves that e.g. made the cable prone to drifting. In general, the resistivity along the profiles mainly changes along the horizontal axis. Changes in resistivity, due to changes in layering, is usually expected along the vertical axis in sedimentary environments. The changes are abrupt with depths, e.g. as in figure 23, with three 'blocks' of resistivity from 20 to more than 63 Ωm towards the NE-end, closest to the river mouth. Figure 26 is an exception, where some horizontal layers are present in depths below 12 meters.

Profile p1 and p3 (figure 22 and 23) are collected near each other, and they show some similarities. The resistivity is increasing from NE to SW in both profiles, with resistivity values in the same range in similar areas in horizontal direction. Profile p6 (figure 24), collected a bit further SE (figure 15) show the same features in the inverse model resistivity of more than 20 Ωm in the NE end of the profile. In profile p9 (figure 25) all resistivity values are less than 0.6 Ωm . The estimated bathymetry of the delta gradient is present in the profile, but the low resistivity values are likely caused by the profile being too short or too deep for the injected current. Profile s4 (figure 27) is similar, in addition to the disturbances in the top 25 meters of the profile. The low resistivity values less than 0.2 Ωm observed at the bottom of the profile does not really give any reliable information.

Some of the lines were too short in combination with the fjord being too deep, with more than 60 meters depth SW of Revet and Hvittensand (figure 15, appendix C). The length of the profile, electrode spacing and the depths of the water is something to consider when using waterborne ERT (Crook & Rucker, 2017; Dahlin et al., 2014). E.g. will depths below 20 meters require electrode spacing that are further apart from each other than 15 meters (Crook & Rucker, 2017). In the survey by Crook & Rucker (2017), it is believed that an electrode spacing of 60 meters is required to be able to map depths of 50 meters. The current lines between the current electrodes and potential electrodes are dependent on the total length of the ERT profile when measurements are carried out in deep water. The current lines between the floating electrodes should reach the seabed (and preferably deeper layers) to get resistivity measurements of sediments, not just the waterbody. In profile p9 and s4 (figure 25 and 27) the

profiles are too short, or the fjord is too deep. Further east, towards the river mouth of Numedalslågen, the water is shallower and the collected lines p1 – p6 (figure 22-24) are longer. Processing of these lines gave a better signal of the measurements, and higher differences in resistivity values.

Another limitation of the method is the sensitivity of the measurements if the cable is drifting due to wind or waves. This gives a curvature of the streamer, but the lines should be kept straight for optimal data collection. When the external GPS was used in addition and positions of electrode are based on estimates from the external GPS data, the inaccuracy of electrode positions increases. This is also affected by lack of detailed bathymetry data, which gives an uncertainty for all directions concerning spatial distribution.

To improve the quality of the ERT profiles, the maximum measured conductivity value (which, as previously mentioned, equals $0.27 \Omega\text{m}$) was set as a standard value for the water body in all processed ERT profiles. Thousands of points with conductivity measurements were collected by the Levelogger. However, these data points were collected at approximately 1 meter depth in the water. In addition, referencing all ERT data points with the measured conductivity values is a nearly impossible job. High variations in conductivity measurements can be caused by variations in temperature or concentrations of salts in the waterbody. The trends of temperature and conductivity distribution in figure 16 show increasing conductivity values with increasing distance from the river mouth. The temperatures also show some trends, with high temperatures between 6.5 and 8.7 °C close to the river mouth and SE of Hvittensand. Between Hvittensand and Revet, there are some colder temperatures (4 to 5 °C). The pattern of the resistivity values could reflect the water discharging from Numedalslågen. Low conductivity values are dominant between Hvittensand and Revet, but they increase towards the fjord. SW of Revet and SE of Hvittensand, on each side of the low resistivity values from the discharging river, higher values are observed (figure 16). The conductivity values plotted in profile p1 and p3 (figure 22 and 23) show a decrease in conductivity that may correlate with the increase in resistivity values in SW to NW direction. However, it is difficult to determine as the resistivity values are varying. In addition, the number of measured conductivity points is relatively low per profile. The conductivity can also be affected by differences in bathymetry of the delta. Variations in bathymetry can give pockets with varying concentrations of salinity or temperature, which is reflected in high or low conductivity.

Regardless of corrections with bathymetry and resistivity of the waterbody, the RMS errors are high for all the processed ERT lines. This could be caused by noise affecting the data, wrong estimates of the depth to the seabed or 3D effects that cannot be solved with the 2D program (Bazin, 2018 (personal communication)). Robust inversion was also applied for some of the profiles, but this did not give any noticeable improvements, with RMS-errors typically 1 % lower than the data presented here. Noise can be one reason for the poor quality of the data. Failures during the surveys, e.g. breaks in the cable or poor ground contact “such that sufficient current cannot be injected into the ground” can cause systematic noise (Loke, 2016). The spikes in figure 17 could be caused by systematic noise. According to Orlando (2013), based on a survey where different electrode configurations were compared, the choice of electrode configuration can affect the results. A dipole-dipole configuration seems more unstable and “to be very sensitive to accuracy of apparent resistivity values and a priori information of the water” (Orlando, 2013). On the other hand, the dipole-dipole array was a good choice considering the possibility of getting high resolution data.

It is difficult to interpret the data and correlate the measured resistivity values with expected sediments in the delta. Horizontal layers in the profiles are absent, instead the resistivities change abrupt in vertical sections. Several of the profiles, e.g. line p1 and p3 are collected less than 100 meters apart from each other, but they still give different results. The structures in the ERT data are not reliable with the high RMS and in lack of horizontal patterns is it impossible to estimate depths to the bedrock or qualify sediment types. Profile s1 (figure 26) have some horizontal layers, with 63 Ωm in the middle of the profile at 18 meters depth, surrounding resistivity values of 20 Ωm and a ‘layer’ of 6 Ωm toward the NW end of the profile at 30 meters depth. However, this cannot be interpreted due to the high RMS statistic, few data points, depths and a general low reliability of the results. To improve the quality of the ERT data, the geometry needs improvement. This requires detailed information about the seabed and extraction of the water depth of each electrode position.

Based on the geomorphological history of the area, the expected sediments in a delta are fluvial sand and marine clays. The starting resistivity value added to the files is 0.2 Ωm , and this represents the waterlayer of the ERT profiles. This value is representative for salt water (figure 7). The dominant and recurring resistivity in the profiles are mainly in the range from 2 Ωm to values between 20 and 63 Ωm . The results referred to in table 1 mainly reports clay rich layers to have resistivity lower than 50 Ωm , depending on composition and consolidation of the layers. The resistivity of sand is expected to be higher than the clay layers, but it is hard

to compare and interpret the values from our ERT results with the results in table 1 and figure 7. In addition, ERT data from several of the publications in table 1, were compared to sedimentary cores which makes it easier to correlate and determine the resistivity values as specific deposits or composition of the soils.

The map in appendix B show water depths of approximately 2 meters in the delta area between Revet and Hvittensand. Old bathymetry data from Kartverkets WMS have shown that the real depths could be up to 6 meters near Revet. Resistivity changes in the top ten meters in the profiles could mean that the topography lines in figure 22-24 reflects the real bathymetry. However, the varying discharge from Numedalslågen will affect erosion and re-deposition of the sediments and the delta top is considered dynamic with continuously changes. Thus, the white lines sketched on the ERT profiles are just an estimate of the water depths based on bathymetry data and variations in resistivity.

The ERT data should (if possible) be combined with other data, as knowledge about the geomorphology, sub bottom maps and cores from drilling. This way resistivity values can be interpreted in combination with other information about an area. As the method is a non-invasive geophysical method, it is suitable for use in vulnerable aquatic environments. It does not affect geological structures in the subsurface, and considering vulnerable ecological sites, it will affect the ecosystems to a minimal degree. Continuous resistivity profiling, CRP, requires a boat to tow the cable. Depending on depths of the water and the motor of the boat, noise and the vortices created from the motor or the bow of the boat at very shallow depths could make an impact on ecology. Some impact on sediments and vegetation is might expected of ERT with cables stationary submerged or dragged along the bottom.

5.3 Discussion GPR data

The GPR data gave varying results, which resulted in a decision of not including all profiles in the results (see appendix D). The profiles from Hvittensand (figure 29) are kept, as GPR line 00 – 02 (figure 30-32) are less noisy. They all show strong reflections in the top layer, between 0 and -2 meters. This is probably the direct signal between the GPR antennas, partly concealing the surface beach sand deposits at Hvittensand. Reflection free parts below the top reflection in the GPR profiles can be caused by saline or brackish groundwater, e.g. as in the NW part of GPR line 00 and SW part of GPR line 01. This seems likely considering the short distance to the fjord and discharging river. With exception of the reflected signals in the top layer of this profile, the GPR signal in general penetrates with a depth of approximately 20 for figure 30-32. At depths below 20 meters, the signal is lost.

Reflection free configurations (figure 12) can be caused by attenuated energy, silty lacustrine sediments, or massive, thick beds of sand or till (Beres & Haeni, 1991). As already mentioned, a penetration depth of 20 meters is the deepest the GPR reaches at Hvittensand. When comparing the profiles directions and reflected signals from the subsurface with the observations from Hvittensand, the reflections towards the North in figure 31 and figure 32 could be an extension of the bedrock outcrop observed in the surface. From figure 29, the reflections in the S end of GPR profile 02 (figure 32) could also be caused by bedrock, as outcrops are present on each side of the profile. The possibility for this layer being clay rich sediments is also present. With higher sea levels after the last glaciation presence of marine clays should be expected. Bedrock, clay and sand all have different geophysical characteristics, but it is very difficult to determine whether it is clay or bedrock below the sand. The same applies to the age and structures of the fluvial deposits, as variations in discharge and relatively frequent flooding of Numedalslågen is expected to affect the structures. The reflection loss is likely caused by presence of clay in the sediments, but it is impossible to interpret if the signal loss is caused by clay layers, brackish groundwater or sediments with fluvial deposits strongly mixed with clays.

GPR line 02 in figure 32 show several reflections below the strong reflection which is interpreted as a bedrock. This interpretation is supported by the observation of bedrock outcrops from the study area. One hyperbola is present in the N part of the profile, and the reflections below the strongest reflection is interpreted to be noise. Another option could be that this strong reflection is a clay rich layer, e.g. with high concentrations of salt in it. The

reflected signal in the S part of GPR line 02 may also be affected by bedrock, as the profile is collected close to bedrock outcrops (figure 29).

Recognizable structures like hummocky, partly wavy reflections or parallel simple layered lines in are all interpreted as sand or deposits containing sand in combination with silt or gravel in figure 12 (Beres & Haeni, 1991). Assumptions based on the possible interpretations in combination with the quaternary map in figure 4, give reason to believe that the sediments mainly can be interpreted as sand, or sand and high amounts of clay.

The strong reflection from the GPR signal penetrating the surface is present in all GPR profiles, including the ones in appendix B. These profiles also have several disturbances appearing along the lines, at varying depths. Because of disturbances of the signals in the profiles in line 03 – 06, they were moved to appendix B. The GPR signal in the profile from Revet is very noisy, and this can be caused by material from the foundations in the ground or lamp posts. The first meters in the SE give a good demonstration of the reflection from concrete, where the signal will not penetrate to underlying sediments or structures (Saarenketo, 2009). The area below the concrete is reflection free. The expected natural materials of Revet is mainly fluvial deposits, when comparing the old maps and development of Revet in appendix B. Revet seems to have built up the NW side of the Numedalslågen delta, but now it is changed with developments and expansions of Revet. The GPS signal penetrates deeper at Revet compared to Hvittensad, but the quality is poorer. The same goes for the profiles further north in Numedalslågen. The reflections in the profiles from Elveveien, Skreppestad and Orøya make interpretations difficult. However, salts in soils are prone to increase the conductivity and create disturbances (Doolittle & Butnor, 2009), which can be an explanation for the Skreppestad profile (surroundings like fields/agricultural land). The profile of Orøya is very noisy, considering the distance from the sea. Saline or brackish groundwater is not expected by Orøya. However, the GPR signal transfer below 15 meters is decreased drastically and could possibly be caused by lenses of clay or clay rich sediments.

5.4 Geology and risk of erosion

Based on assumptions from general knowledge about hydrology and sedimentary geology, expected sediments in the delta are fluvial sand and marine clays. The content and distribution of sand and clay depends on river dynamics like volume discharge. An increase in snowmelt and rainfall is likely to increase the discharge of the river, which increases the erosion risk. The risk of erosion at Hvittensand and in the top layer of the delta should be considered as likely with a sudden increase in discharge. Tides, seasonal changes in sea levels and storm surges can also affect erosion and re-deposition of the sand of Hvittensand. A comparison of figure 16 and 29 with appendix B and C also show changes in the extent of Hvittensand and the spit. Especially the map in figure 29 illustrate this, as the extent of the beach stretched several meters further NE when the GPR lines were collected. It is difficult to discuss erosion risk in the delta any further based on the ERT results. With adjustments and improvements of bathymetry data the profiles could have been used to make a 3D model or a survey grid (e.g. as in Epting et al. (2012)). This could have provided information about the delta top and used to calculate estimates of the delta gradient. A 3D survey grid could also possibly have been used to analyse trenches, flow patterns and erosion risk based on sediments, currents and gradient, or alternatively to plan further bathymetry surveys or geophysical investigations. It is important to be aware of the temporal changes of the delta top and continuously changing bathymetry.

6. Conclusion

The data collected with electrical resistivity tomography gave results which were difficult to interpret. The vertical sections of resistivity changes in the profiles in combination with high RMS statistics made it impossible to determine thickness of sediments and the depth to bedrock. The resistivity values ranging from 20 – 60 Ωm is interpreted to be clay. If more detailed bathymetry data were available, the resistivity data could possibly be used to interpret thickness or layering of the sediments or combined in a 3D grid. However, the survey was a good opportunity to test waterborne ERT as a method and the challenges with it. The ground penetrating radar profiles were also challenging to interpret. The penetration depth of the GPR were maximum 20 meters. Several parts of the profiles were reflection free, indicating clay rich sediments or sediments with brackish groundwater. Wavy and hummocky structures were interpreted as bedded sand.

7. References

- Bazin, S. (2018). *Discussion of waterborne ERT data and method* (Personal communication).
- Befus, K. M., Cardenas, M. B., Tait, D. R. & Erler, D. V. (2014). Geoelectrical signals of geologic and hydrologic processes in a fringing reef lagoon setting. *Journal of Hydrology*, 517: 508-520. doi: <https://doi.org/10.1016/j.jhydrol.2014.05.070>.
- Beres, M. & Haeni, F. P. (1991). Application of Ground-Penetrating-Radar Methods in Hydrogeologic Studies. *Groundwater*, 29 (3): 375-386. doi: doi:10.1111/j.1745-6584.1991.tb00528.x.
- Berthelsen, A. & Sundvoll, B. (1996). *Berggrunnskart Oslo M 1:250 000*: Norges Geologiske Undersøkelse.
- Breier, J. A., Breier, C. F. & Edmonds, H. N. (2005). Detecting submarine groundwater discharge with synoptic surveys of sediment resistivity, radium, and salinity. *Geophysical Research Letters*, 32 (23). doi: 10.1029/2005GL024639.
- Bristow, C. S. & Jol, H. M. (2003). An introduction to ground penetrating radar (GPR) in sediments. In Bristow, C. S. & Jol, H. M. (eds) *Ground Penetrating Radar in Sediments*: Geological Society of London.
- Cardenas, M. B., Zamora, P. B., Siringan, F. P., Lapus, M. R., Rodolfo, R. S., Jacinto, G. S., San Diego-McGlone, M. L., Villanoy, C. L., Cabrera, O. & Senal, M. I. (2010). Linking regional sources and pathways for submarine groundwater discharge at a reef by electrical resistivity tomography, ^{222}Rn , and salinity measurements. *Geophysical Research Letters*, 37 (16): n/a-n/a. doi: 10.1029/2010GL044066.
- Cassiani, G., Bruno, V., Villa, A., Fusi, N. & Binley, A. (2006). A saline trace test monitored via time-lapse surface electrical resistivity tomography. *Journal of Applied Geophysics*, 59 (3): 244-259. doi: <https://doi.org/10.1016/j.jappgeo.2005.10.007>.
- Clémence, H., Marc, P., Véronique, D. & Tohir, A. (2017). Monitoring an artificial tracer test within streambed sediments with time lapse underwater 3D ERT. *Journal of Applied Geophysics*, 139: 158-169. doi: <https://doi.org/10.1016/j.jappgeo.2017.02.003>.
- Colombero, C., Comina, C., Gianotti, F. & Sambuelli, L. (2014). Waterborne and on-land electrical surveys to suggest the geological evolution of a glacial lake in NW Italy. *Journal of Applied Geophysics*, 105: 191-202. doi: <https://doi.org/10.1016/j.jappgeo.2014.03.020>.

- Crook, N., Binley, A., Knight, R., Robinson, D. A., Zarnetske, J. & Haggerty, R. (2008). Electrical resistivity imaging of the architecture of substream sediments. *Water Resources Research*. doi: <https://doi.org/10.1029/2008WR006968>
- Crook, N. & Rucker, F. D. (2017). Waterborne Electrical Resistivity of the Hypersaline Mono Lake. *Journal of Environmental and Engineering Geophysics*, 22 (2).
- Dahlin, T., Loke, M. H., Siikanen, J. & Höök, M. (2014). *Underwater ERT Survey for Site Investigation for a New Line for Stockholm Metro*. 20th European Meeting of Environmental and Engineering Geophysics: EAGE.
- Daily, W., Ramirez, A., Binley, A. & LeBrecque, D. (2004). Electrical resistance tomography. *The Leading Edge*, 23 (5): 438-442. doi: 10.1190/1.1729225.
- Day-Lewis, F. D., White, E. A., Johnson, C. D., Lane Jr., J. W. & Belaval, M. (2006). Continuous resistivity profiling to delineate submarine groundwater discharge—examples and limitations. *The Leading Edge*, 25 (6): 724-728. doi: 10.1190/1.2210056.
- De Blasio, F. V. (2011). Friction, Cohesion, and Slope Stability. In de Blasio, F. V. (ed.) *Introduction to the Physics of Landslides: Lecture notes on the dynamics of mass wasting*, pp. 23-52. Dordrecht: Springer Netherlands.
- Di Prinzio, M., Bittelli, M., Castellarin, A. & Pisa, P. R. (2010). Application of GPR to the monitoring of river embankments. *Journal of Applied Geophysics*, 71 (2): 53-61. doi: <https://doi.org/10.1016/j.jappgeo.2010.04.002>.
- Dons, J. A. & Jorde, K. (1978). *Berggrunnskart Skien. M 1:250 000*: Norges Geologiske Undersøkelse.
- Doolittle, J. A. & Butnor, J. R. (2009). Chapter 6 - Soils, Peatlands, and Biomonitoring. In Jol, H. M. (ed.) *Ground Penetrating Radar Theory and Applications*, pp. 177-202. Amsterdam: Elsevier.
- Eilertsen, R. R., Corner G, D., Aasheim, O. & Hansen, L. (2011). Facies characteristics and architecture related to paleodepth of Holocene fjord-delta sediments. *Sedimentology*, 58 (7).
- Epting, E., Wüest, A. & Huggenberger, P. (2012). Investigating sediments and rock structures beneath a river using underwater ERT. *Central European Journal of Geosciences*, 4 (1): 81-93.
- GeoNorge. (n.d). *Map Catalogue Kartverket*. Available at: <https://kartkatalog.geonorge.no/search> (accessed: 05.06.2018).

- Hanssen-Bauer, I., Førland, E. J., Haddeland, I., Hisdal, H., Lawrence, D., Mayer, S., Nesje, A., Nilsen, J. E. Ø., Sandven, S., Sandø, A. B., et al. (2017). *Climate in Norway 2100 - a knowledge base for climate adaption*. Miljødirektoratet: Miljødirektoratet.
- Harbitz, C. B., Frauenfelder, R., Glimsdal, S., Høydal, Ø. A., Kaiser, G., L'Heureux, J.-S., Ekseth, K. H. H. & Sandersen, F. (2016). *Lardal og Larvik kommuner - tilpasninger til klimaendringer*. : NGL.
- Holtebekk, T. (2017). *Store norske leksikon: Resistivitet*. Store Norske Leksikon: Store Norske Leksikon. Available at: <https://snl.no/resistivitet> (accessed: 29.01).
- Huntley, D., Bobrowsky, P. & Best, M. (2017). *Combining Terrestrial and Waterborne Geophysical Surveys to Investigate the Internal Composition and Structure of a Very Slow-Moving Landslide Near Ashcroft, British Columbia, Canada*, Cham: Springer International Publishing.
- Jaksland, L. (2014). Kulturhistorisk sammenstilling. In Jaksland, L., Persson, P. (ed.) vol. E18 Brunelanesprosjektet bind I. Forutsetninger og kulturhistorisk sammenstilling. *Varia* 79.
- Jørgensen, P. & Sørensen, R. (1979). Late Glacial and Holocene deglaciation and sedimentation in Lågendalen, southeastern Norway. *Norwegian Journal of Geology*, 59 (4): 337-343.
- Jørgensen, P., Sørensen, R. & Haldorsen, S. (1997). *Kvartærgeologi*. 2nd ed.: Tun Forlag.
- Jørgensen, P., Sørensen, R. & Prestvik, O. (2013). *Norske jordarter*. Bioforsk. Available at: http://www.bioforsk.no/ikbViewer/Content/114780/Norske_jordarter.pdf (accessed: 09.02.2018).
- Kartverket. (n.d. a)). *Sjøkart*. Available at: http://www.norgeskart.no/?&_ga=2.258822730.1312461649.1525071506-917382396.1510748717#!?zoom=13&lon=217164.89&lat=6554582.76&project=dekning&layers=1008 (accessed: 14.03.2018).
- Kartverket. (n.d. b)). *Water level and tidal information*: Kartverket. Available at: <https://www.kartverket.no/en/sehavniva/Lokasjonsside/?cityid=720298&city=Hvittensand#tab2> (accessed: 10.05.2018).
- Knödel, K., Krummel, H. & Lange, G. (1997). *Handbuch zur Erkundung des Untergrundes von Deponien und Altlasten. Band 3: Geophysik*.
- Loke, M. H. (2016). *Tutorial: 2-D and 3-D electrical imaging survey*: Geotomo Software. Available at: <http://www.geotomosoft.com/downloads.php> (accessed: 26.10.2017).

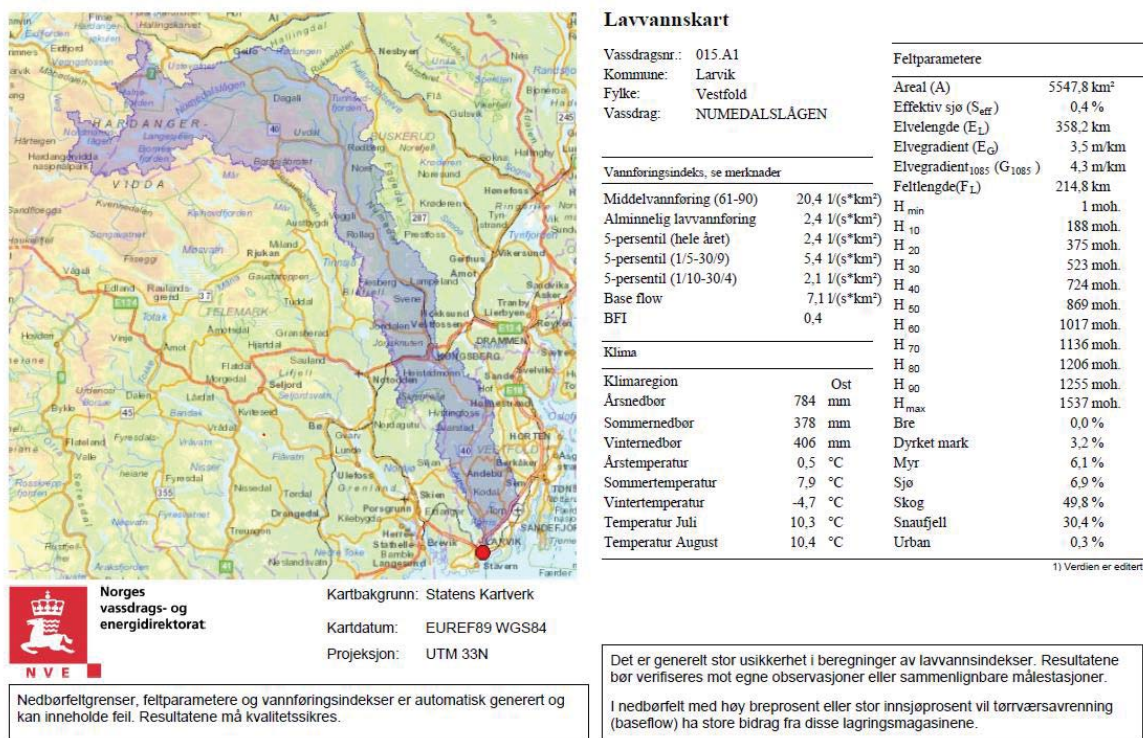
- Loke, M. H. (n.d). *Geoelectrical Imaging 2D & 3D*: GeotomoSoftware. Available at: <http://www.geotomosoft.com/> (accessed: 14.11.2018).
- Maillet, G. M., Rizzo, E., Revil, A. & Vella, C. (2004). High Resolution Electrical Resistivity Tomography (ERT) in a Transition Zone Environment: Application for Detailed Internal Architecture and Infilling Process Study of a Rhône River Paleo-channel. *Marine Geophysical Researches*, 26 (2-4).
- Mauringer, E., Koziel, J., Lauritsen, T., Rønning, J. S. & Tønnesen, J. F. (1996). *Målinger med georadar. Teori, anvendelse, teknikker og eksempler på opptak*: Norges Geologiske Undersøkelse.
- Neal, A. (2004). Ground-penetrating radar and its use in sedimentology: principles, problems and progress. *Earth-Science Reviews*, 66 (3): 261-330. doi: <https://doi.org/10.1016/j.earscirev.2004.01.004>.
- NGI. (n.d.). *MERRIC: WP4 - Monitoring, warning and non-physical mitigation measures*. Available at: <https://www.ngi.no/eng/Projects/MERRIC/WP4-Monitoring-warning-and-non-physical-mitigation-measures> (accessed: 01.02.2018).
- NGU. (n.d). *Sediments - Quaternary Geology. WMS Service*. Available at: <http://geo.ngu.no/mapserver/LosmasserWMS> (accessed: 06.06.2018).
- Norsk Klimaservicesenter. (2015). *Klimaprofil Vestfold. Et kunnskapsgrunnlag for klimatilpasning*. . Available at: <https://cms.met.no/site/2/klimaservicesenteret/klimaprofiler/klimaprofil-vestfold/attachment/12098?ts=15ea344ee93>.
- NVE. (2010). *Vassdragshåndboka*: Tapir Forlag.
- NVE. (n.d.). *NEVINA: Nedbør-Vannføring-INdeks-Analyse*: NVE. Available at: <http://nevina.nve.no/> (accessed: 29.01).
- Nyquist, J. E., Freyer, P. A. & Toran, L. (2008). Stream Bottom Resistivity Tomography to Map Ground Water Discharge. *Groundwater*, 46 (4): 561-569. doi: doi:10.1111/j.1745-6584.2008.00432.x.
- Olsen, K. S. & Løwe, A. (1984). *Sandefjord 1813 III, kvartærgeologisk kart - 1:50 000*: Norges Geologiske Undersøkelse.
- Orlando, L. (2013). Some considerations on electrical resistivity imaging for characterization of waterbed sediments. *Journal of Applied Geophysics*, 95: 77-89. doi: <https://doi.org/10.1016/j.jappgeo.2013.05.005>.
- Palacky, G. J. (1987). Clay mapping using electromagnetic methods. *First Break*, 5: 295-306.

- Passaro, S. (2010). Marine electrical resistivity tomography for shipwreck detection in very shallow water: a case study from Agropoli (Salerno, southern Italy). *Journal of Archaeological Science*, 37 (8): 1989-1998. doi: <https://doi.org/10.1016/j.jas.2010.03.004>.
- Rucker, D. F., Noonan, G. E. & Greenwood, W. J. (2011). Electrical resistivity in support of geological mapping along the Panama Canal. *Engineering Geology*, 117 (1): 121-133. doi: <https://doi.org/10.1016/j.enggeo.2010.10.012>.
- Saarenketo, T. (2009). Chapter 13 - NDT Transportation. In Jol, H. M. (ed.) *Ground Penetrating Radar Theory And Applications*, pp. 395-444. Amsterdam: Elsevier.
- Schwartz, F. W. & Zhang, H. (2003). *Fundamentals of ground water* John Wiley & Sons, Inc.
- Sebok, E., Karan, S. & Engesgaard, P. (2018). Using hydrogeophysical methods to assess the feasibility of lake bank filtration. *Journal of Hydrology*. doi: <https://doi.org/10.1016/j.jhydrol.2018.04.049>.
- Sensors and Software Inc. (2016). *EKKO_Project. LineView & Interpretation Modules. User's Guide*.
- Sensors and Software Inc. (2017). *EKKO_Project. User's Guide*.
- Sharma, P. V. (1997). *Environmental and engineering geophysics*: Cambridge University Press.
- Sigmond, E. M. O. (1998). *Berggrunnskart Odda. M 1:250 000*: Norges Geologiske Undersøkelse.
- Swarzenski, P. W., Kruse, S., Reich, C. & Swarzenski, W. V. (2007). Multi-channel resistivity investigations of the freshwater-saltwater interface: a new tool to study an old problem. *Indian Journals*, 17 (4).
- Sørensen, R., Høeg, H. I., Henningsmoen, K. E., Skog, G., Labowsky, S. F. & Stabell, B. (2014). Utviklingen av det senglasiøle og tidlige preboreale landskapet og vegetasjonen omkring steinalderboplassen ved Pauler, Larvik kommune, Vestfold. In Jaksland, L., Persson, P. (ed.) vol. E18 Brunlanesprosjektet bind I. Forutsetninger og kulturhistorisk sammenstilling. *Varia* 79.
- Sørensen, R., Grønlie, G., Jørgensen, P. (1982). Thickness and layering of the Odbergmoen Late Weichselian and Holocene sediments in Lågendalen, southeastern Norway. *Norwegian Journal of Geology*, 62 (1): 7-15.

- Thorsnæs, G. & Heggstad, R. (2017). *Store norske leksikon: Numedalslågen*. Store Norske Leksikon: Store Norske Leksikon. Available at: <https://snl.no/Numedalsl%C3%A5gen> (accessed: 09.02.2018).
- Tucker, M. E. (1991). *Sedimentary Petrology. An Introduction to the Origin of Sedimentary Rocks*. 2nd ed.: Blackwell Scientific Publications.
- Vandenberghe, J. & van Overmeeren, R. A. (1999). Ground penetrating radar images of selected fluvial deposits in the Netherlands. *Sedimentary Geology*, 128 (3): 245-270. doi: [https://doi.org/10.1016/S0037-0738\(99\)00072-X](https://doi.org/10.1016/S0037-0738(99)00072-X).
- Økland, J. & Økland, K. A. (2006). *Vann og vassdrag 3. Kjemi, fysikk og miljø*. 2 ed.: Forlaget Vett & Viten.

8. Appendices

Appendix A: Catchment of Numedalslågen



Flomberegning

Vassdragsnr.: 015.A1
Kommune: Larvik
Fylke: Vestfold
Vassdrag: NUMEDALSLÅGEN

Resultat er kun validert for areal mindre enn 60km².
Flomestimatene er derfor nødvendigvis ikke gyldige.

Flomverdiene viser størrelsen på kulminasjonsflommer for ulike gjentakintervall. De er beregnet ved bruk av et formelverk som er utarbeidet for nedbørfelt under ca 50 km². Feltparametere som inngår i formelverket er areal, effektiv sjøprosent og normalavrenning (l/s*km²). For mer utdypende beskrivelse av formelverket henvises det til NVE –Rapport 7/2015 «Veileder for flomberegninger i små uregulerte felt». Det pågår fortsatt forskning for å bestemme klimapåslag for momentanflommer i små nedbørfelt. Frem til resultatene fra disse prosjektene foreligger anbefales et klimapåslag på 1.2 for døgnmiddelflom og 1.4 for kulminasjonsflom i små nedbørfelt.

NUMEDALSLÅGEN

Areal (km ²)	5547,83
Klimafaktor	1,4

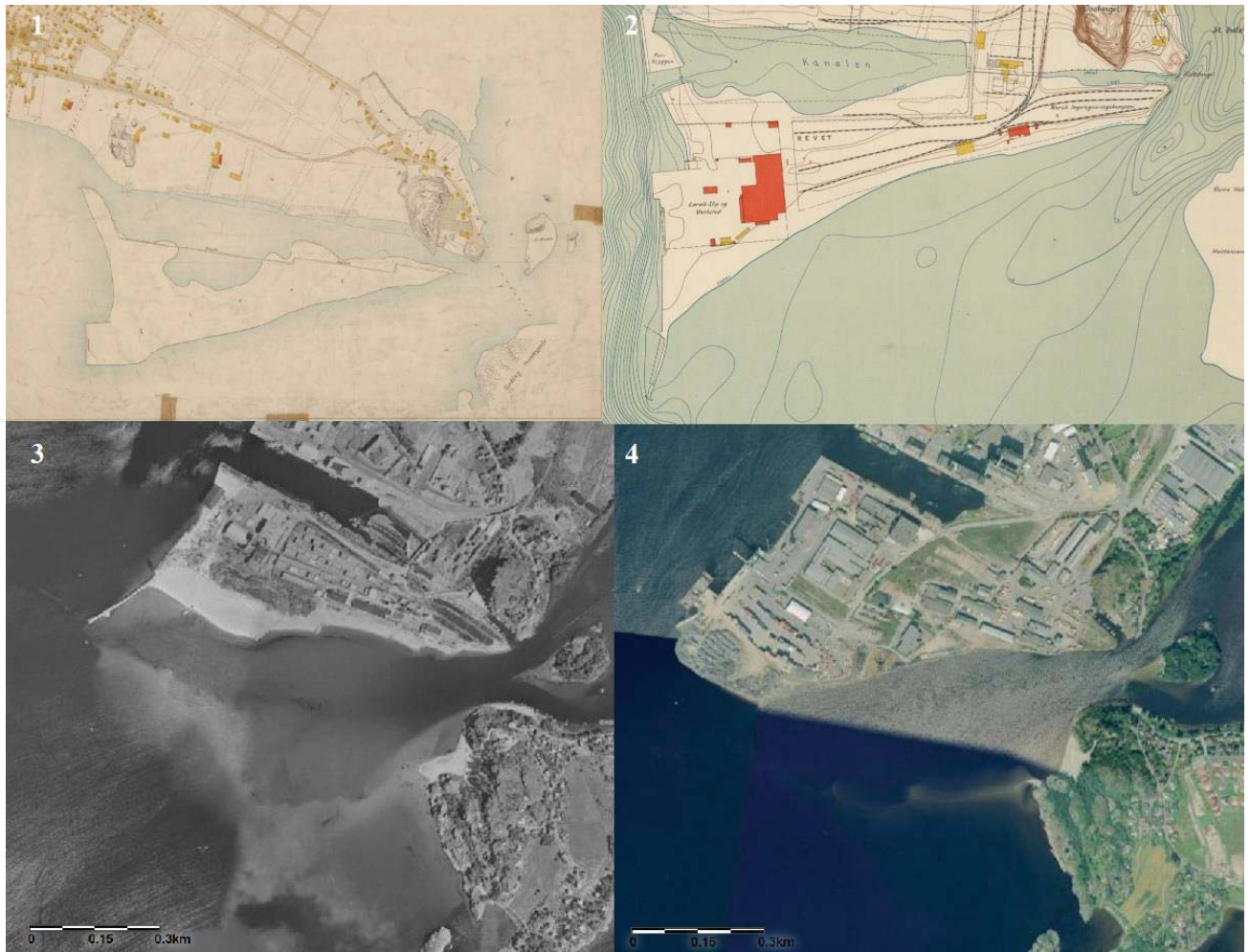
	Q ^M		Q ⁵	Q ¹⁰	Q ²⁰	Q ⁵⁰	Q ¹⁰⁰	Q ²⁰⁰
	m ³ /s	l/(s*km ²)						
Flomfrekvensfaktorer	-	-	1,26	1,49	1,75	2,12	2,46	2,83
95% intervall øvre grense (m ³ /s)	1665,8	300,3	2140,4	2598,2	3104,5	3898,8	4621,2	5330,2
Flomverdier (m ³ /s)	941,1	170	1182,6	1404,4	1642,6	1999,4	2310,6	2665,1
95% intervall nedre grense (m ³ /s)	531,7	96	653,3	759,1	869,1	1025,3	1155,3	1332,6
Flommer med klimapåslag (m ³ /s)	1317,6	237,5	1182,6	1966,2	2299,6	2799,1	3234,8	3731,1

Beregningene er automatisk generert og kan inneholde feil. Det er generelt stor usikkerhet i denne typen beregninger. Resultatene må verifiseres mot egne observasjoner eller sammenlignbare målestasjoner. Resultatene er ikke gyldig som grunnlag til flomberegninger for klassifiserte dammer.

© nevina.nve.no

Catchment and hydrological parameters of Numedalslågen. From NEVINA, NVE. Available at <http://nevina.nve.no> (accessed the 29.01.18).

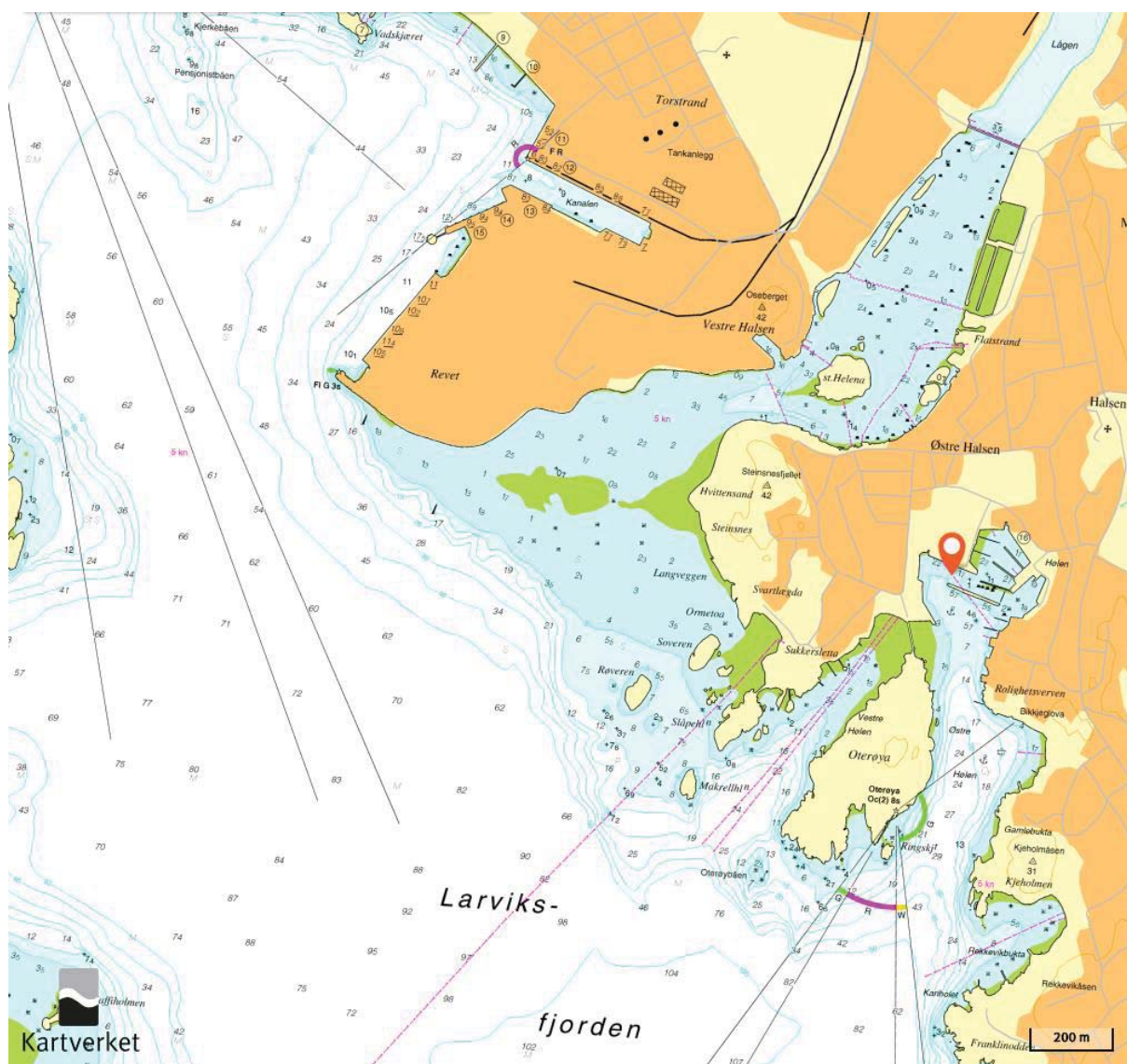
Appendix B: The development of Revet



Old maps and aerial photos of Revet and Hvittensand, showing changes and development.

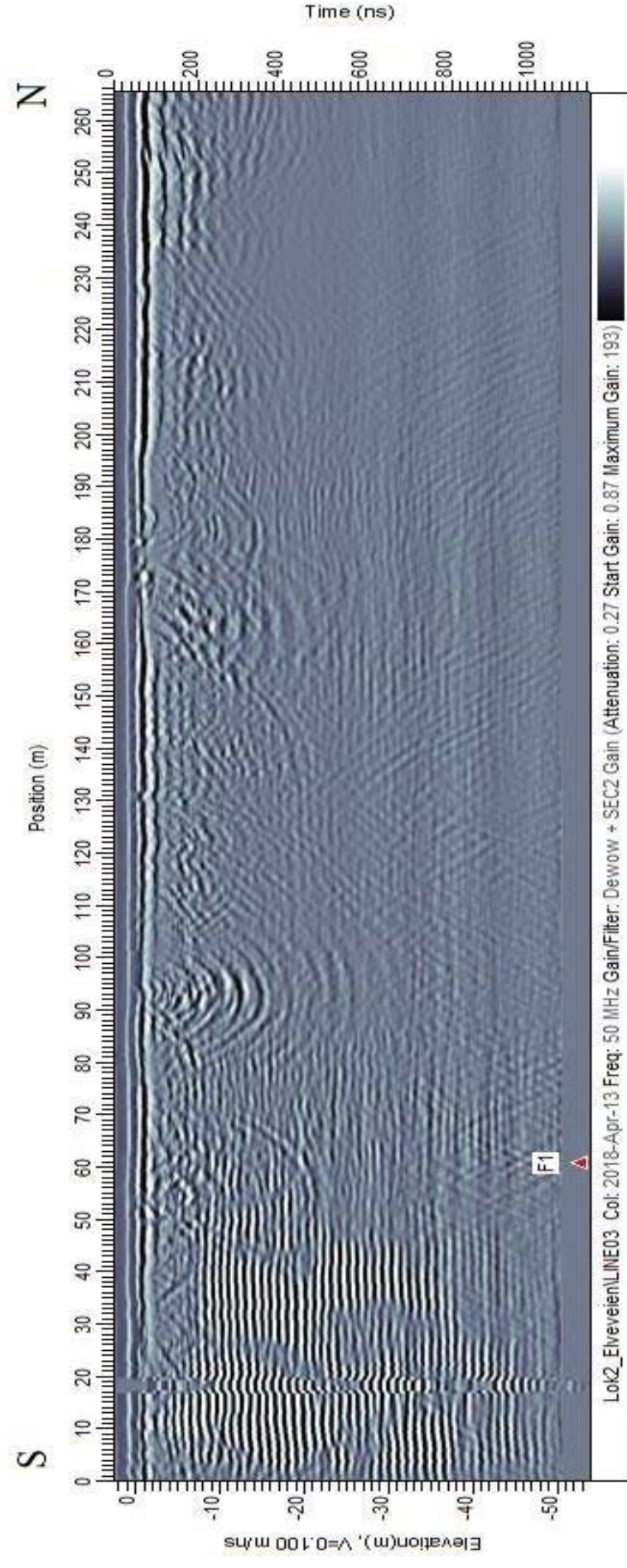
1. Laurvig 1884. Retrieved 10th of may 2018 from Kartverket:
https://www.kartverket.no/historiske/amt2/jpg100dpi/amt2_jarlsberg-og-larviks-amt-44-oest_1884.jpg
2. Jarlsberg og Larviks amt Øst 1927. Retrieved the 10th of May 2018 from Kartverket:
<http://www.norgeskart.no>
3. Vestfold 1959 – 1959. Retrieved the 10th of may 2018 from Norge i bilder:
<http://www.norgeibilder.no/?x=216629&y=6554819&level=13&utm=33&projects=770&layers=&planned=0>
4. Vestfold 2002. Retrieved the 10th of May 2018 from Norge i bilder:
<http://www.norgeibilder.no/?x=216265&y=6554819&level=13&utm=33&projects=771&layers=&planned=0>

Appendix C: Nautical chart of study area

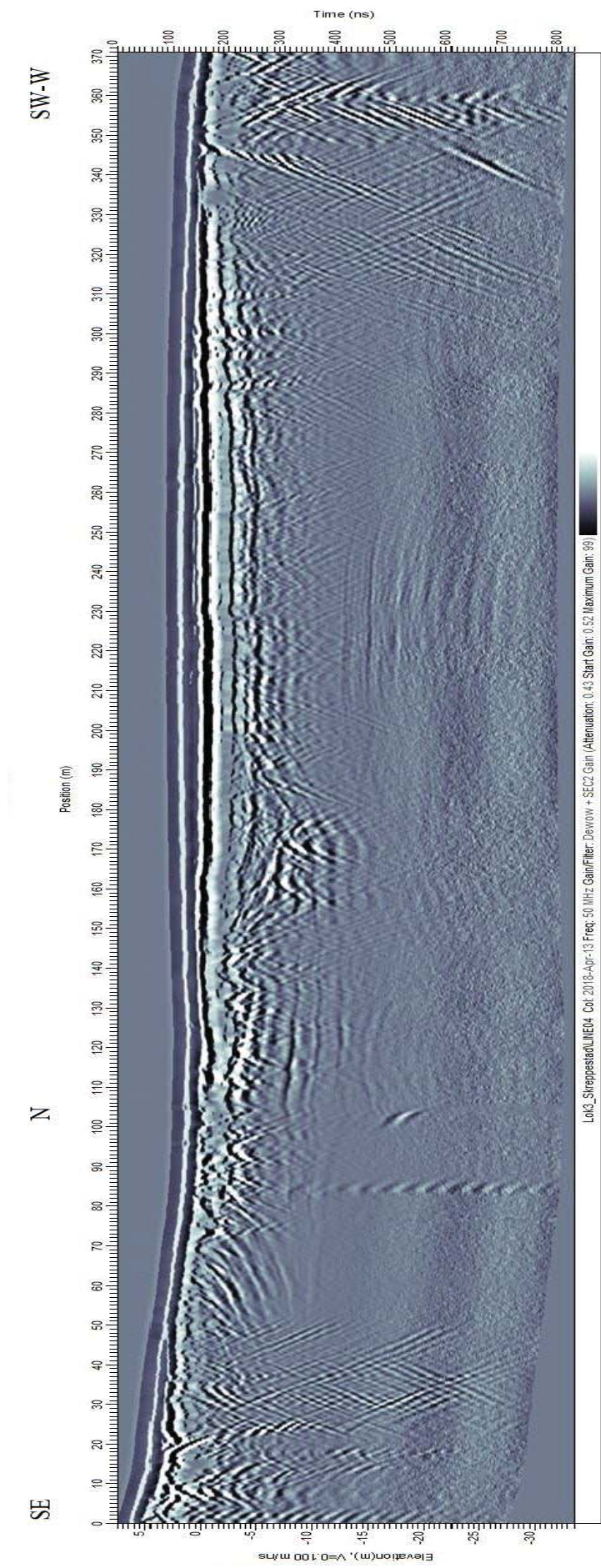


Nautical chart of the study area. Retrieved the 30th of April 2018 from Kartverket:
http://www.norgeskart.no/?&_ga=2.258822730.1312461649.1525071506-917382396.1510748717#!?zoom=13&lon=217164.89&lat=6554582.76&project=dekning&layers=1008

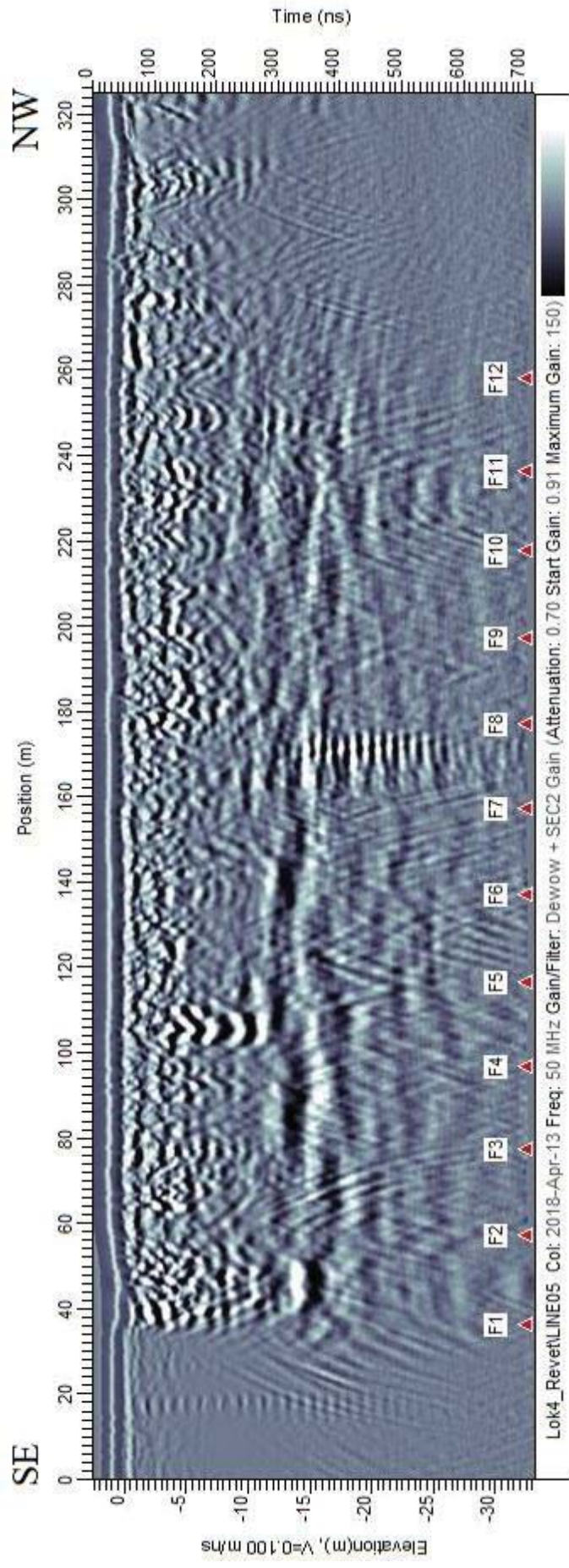
Appendix D: GPR profiles



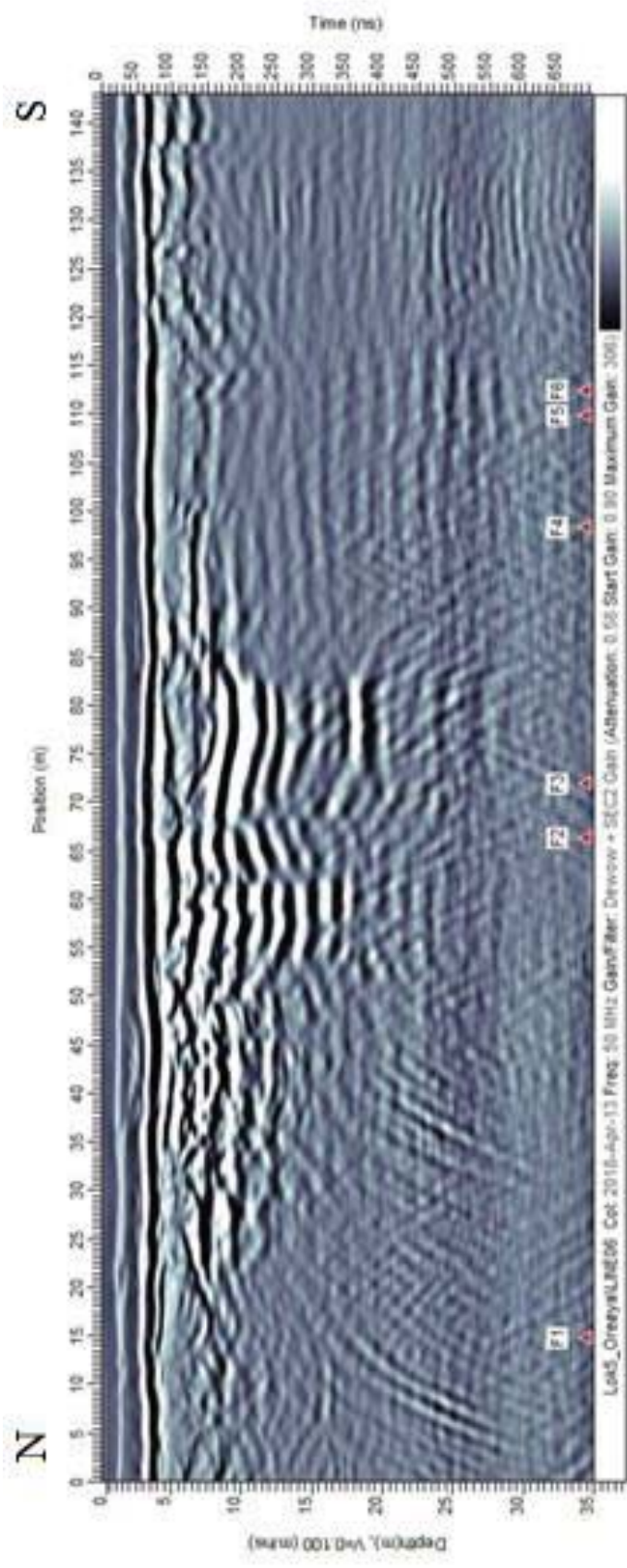
GPR line 03, profile from Elveveien. F1 marks the position of a well.



GPR line 04, profile from Skreppestad. SE to N to SW-W direction from left to right:



GPR line 05, profile from Revet. F1-F12 mark position of lamp posts.



GPR line 06, profile from Orøya. The path was covered by snow and ice between F1 and F2, F3 and F4 and F5 and F6.



Norges miljø- og biovitenskapelige universitet
Noregs miljø- og biovitenskapelige universitet
Norwegian University of Life Sciences

Postboks 5003
NO-1432 Ås
Norway